Part II
Electronic and Magnetic Applications

Chapter 6
Development of Hybrid Nanocomposites for Electronic Applications

S.K. Samudrala and Sri Bandyopadhyay

Abstract Hybrid inorganic–organic nanocomposite materials with their widely varying electrical and mechanical properties offer promising applications in many areas of the electronic industry and have been traditionally employed as insulators and dielectrics. The development of new materials has broadened their utilization into areas where their semi-conducting and conducting properties have encouraged use in many novel applications. In this chapter we have reviewed on the material aspects of nanocomposites used in the following electronic applications: integrated circuits, embedded capacitors, transistors, lithium ion batteries, light emitting diodes, information storage, and briefly about liquid crystal, flat panel displays and ultra large scale integrated (ULSI) devices.

6.1 Introduction

Hybrid organic–inorganic materials are nanocomposites with organic and inorganic components that are either homogeneous systems derived from monomers and miscible organic and inorganic components, or heterogeneous systems (nanocomposites) where at least one of the components' domains has a dimension ranging from some Angstrom to several nanometers. The improved or unusual features related to multi-phase structures of these materials not only represent an alternate to design new multifunctional materials and compounds for academic research, but also result in the development of innovative industrial applications [1–3]. These new generations of hybrid materials, offer a land of promising applications in many areas including electronics, ionics, mechanics, energy, environment, biology,

S.K. Samudrala and S. Bandyopadhyay (✉)
School of Materials Science and Engineering, University of New South Wales,
Sydney, NSW 2052 Australia
e-mail: s.bandyopadhyay@unsw.edu.au

L. Merhari (ed.), *Hybrid Nanocomposites for Nanotechnology*,
DOI: 10.1007/978-0-387-30428-1_6,

optics, medicine (for example as separation devices and membranes), functional smart coatings, solar and fuel cells, catalysts, sensors, etc [1, 4–19].

Nanocomposites represent the current trend in novel nanostructured materials. Properties of these materials are not only limited to the sum of the individual contributions of both phases, but also the role of the inner interfaces could be predominant. Based on the nature of the interface, nanocomposites can be divided into two distinct classes [1, 5, 20, 21] where (a) organic and inorganic components are embedded and only weak hydrogen, van der Waals or ionic bonds give the cohesion to the whole structure and (b) the two phases are linked together through strong chemical covalent or iono-covalent bonds.

Nanocomposites being at the interface of organic and inorganic realms offer a wide range of possibilities to elaborate tailor-made materials in terms of processing, chemical and physical properties. Hybrid materials generate smart microelectronic, or intelligent therapeutic vectors that combine targeting, imaging, therapy and controlled release properties. Electronic technologies that allow for a reduction in size, weight, and cost while improving functionality and performance are highly desired for military and commercial applications, including telecommunications, network systems, automotives, and computer electronic devices [1, 4–19]. Hybrid inorganic–organic nanocomposites with their widely varying electrical and mechanical properties have been traditionally employed as insulators and dielectrics but, the development of new materials has broadened their utilization into areas where their semiconducting and conducting properties have encouraged use in many novel applications. This review will focus on the material aspects of nanocomposites used for electronic applications such as: integrated circuits, embedded capacitors, transistors, lithium ion batteries, light emitting diodes, information storage, and briefly about liquid crystal, flat panel displays and ULSI devices. Before going into the review it is appropriate to briefly introduce these applications.

6.1.1 Background

6.1.1.1 Transistors

A transistor is a three-terminal semiconductor device that can be used for amplification, switching, voltage stabilization, signal modulation and many other functions. Transistor is a fundamental building block of both digital and analog integrated circuits. In analog circuits, transistors are used in amplifiers, (direct current amplifiers, audio amplifiers, radio frequency amplifiers), and linear regulated power supplies. Transistors are also used in digital circuits such as logic gates, random access memory (RAM), microprocessors, and digital signal processors (DSPs) where they function as electronic switches.

Transistors are divided into two main categories: bipolar junction transistors (BJTs) and field effect transistors (FETs). The vast majority of transistors are fabricated into integrated circuits (also called *microchips* or simply *chips*) along

with diodes, resistors, capacitors and other electronic components to produce complete electronic circuits. A logic gate comprises about twenty transistors whereas an advanced microprocessor, as of 2006, can use as many as 1.7 billion transistors [22]. Field-effect transistors (FETs), sometimes called unipolar transistors, use either electrons (N-channel FET) or holes (P-channel FET) for conduction. Like bipolar transistors, FETs can be made to conduct with light (photons) as well as voltage. Devices designed for this purpose are called phototransistors.

Transistors have the applications in and as [23–25]:

(1) Electronic Switches: for both high power applications including switched-mode power supplies and low power applications such as logic gates.
(2) Amplifiers: from mobile phones to televisions, vast numbers of products include amplifiers for sound reproduction, radio transmission, and signal processing. Transistors are commonly used in modern musical instrument amplifiers, where circuits up to a few hundred watts are common and relatively cheap. They have largely replaced valves in instrument amplifiers. In some cases of musical instrument amplifiers both transistors and vacuum tubes are used in the same circuit, to utilize the inherent benefits of both the devices.
(3) Computers: development of transistors was the key to computer miniaturization and reliability. Transistors incorporated into integrated circuits have replaced most discrete transistors in modern digital computers.

Some advantages of transistors over conventional vacuum tubes include [1, 5, 12, 22, 26–32]: smaller size, highly automated manufacture, lower cost (in volume production), lower possible operating voltages, no warm-up period, lower power dissipation, higher reliability, longer life, and ability to control large currents.

6.1.1.2 Integrated Circuits

Integrated circuits (ICs) were made possible by technology advancements in semiconductor device fabrication (by mid-twentieth century) and by the experimental discoveries that showed semiconductor devices could perform the functions of vacuum tubes [33–35]. The integration of large numbers of tiny transistors into a small chip was an enormous improvement over the manual assembly of circuits using discrete electronic components. The integrated circuit's mass production capability, reliability, and building-block approach to circuit design ensured the rapid adoption of standardized ICs in place of designs using discrete transistors. There are two main advantages of ICs over discrete circuits: cost and performance. As of 2006, chip areas range from a few square mm to around 250 mm^2, with up to 1 million transistors per mm^2 [22].

Microprocessors are the most advanced integrated circuits, which control computers to cellular phones to digital microwave ovens. Digital memory chips are another family of integrated circuits that are crucially important to the modern information society [36]. While the cost of designing and developing a complex integrated circuit

is quite high, when spread across typically millions of production units the individual IC cost is minimized. Since the speed and power consumption gains are apparent to the end user, there is fierce competition among the manufacturers to use finer geometries [33–35].

Integrated circuits can be classified into analog, digital and mixed signal (both analog and digital on the same chip) [37]. Digital integrated circuits contain from one to millions of logic gates, flip-flops, multiplexers, and other circuits in a few square millimeters [38]. The small size of these circuits allows high speed, low power dissipation, and reduced manufacturing cost compared with board-level integration [39]. In 1986 the first one megabit RAM chips were introduced, which contained more than one million transistors. Microprocessor chips produced in 1994 contained more than three million transistors. The latest server processor from Intel had four billion transistors on a chip [22].

6.1.1.3 Capacitors

Capacitors, (energy-storage devices in electrical circuits) can also be used to differentiate between high-frequency and low-frequency signals which make them useful in electronic filters.

Capacitors have various uses in electronic and electrical systems such as [40–42]:

(a) Energy storage, filtering, signal coupling, noise filters, motor starters,
(b) Signal processing (energy stored in a capacitor can be used to represent information, either in binary form, or in analogue form, as in analog sampled filters),
(c) Tuned circuits (capacitors and inductors are applied together in tuned circuits to select information in particular frequency bands),
(d) Sensor applications [43, 44]:

I. Capacitors with an exposed and porous dielectric can be used to measure humidity in air; by changing the distance between the plates, capacitors can also be used to accurately measure the fuel level in airplanes
II. Capacitors with a flexible plate can be used to measure strain or pressure
III. Capacitors are used as sensors in condenser microphones,
IV. Some accelerometers use MEMS capacitors etched on a chip to measure the magnitude and direction of the acceleration vector
V. They are used to detect changes in acceleration, e.g., as tilt sensors or to detect free fall, as sensors triggering airbag deployment, and fingerprint sensors

6.1.1.4 Lithium Ion Batteries

Lithium (Li) ion batteries are rechargeable batteries that are commonly used in consumer electronics. They are the most popular type of batteries, with one of the

Table 6.1 Permanent capacity loss vs. storage conditions in lithium ion batteries at different temperatures [45]

Storage Temperature (°C)	100% Charge	40% Charge
0	6% loss after 1 year	2% loss after 1 year
25	20% loss after 1 year	4% loss after 1 year
40	35% loss after 1 year	15% loss after 1 year
60	40% loss after 3 months	25% loss after 1 year

best energy-to-weight ratios, no memory effect and a slow loss of charge when not in use. Lithium ion batteries can be formed into a wide variety of shapes and sizes, so as to efficiently fill available space in the devices they power. The forte of the Li-ion chemistry is the high open circuit voltage in comparison to aqueous batteries (such as lead acid, nickel metal hydride and nickel cadmium). However, a unique drawback of the Li-ion battery is its life span that is dependent upon aging from the time of manufacturing regardless of the number of charge/discharge cycles. Table 6.1 [46] lists the permanent capacity loss of Li ion batteries vs. storage conditions at different temperatures.

6.1.1.5 Light Emitting Diodes

Organic light-emitting diodes (OLEDs) are a special type of light-emitting diodes (LEDs) in which the emissive layer comprises a thin-film of certain organic compounds. The emissive electroluminescent layer can include a polymeric substance that allows the deposition of very suitable organic compounds, for example, in rows and columns on a flat carrier by using a simple "printing" method to create a matrix of pixels which can emit different color light [47]. One of the great benefits of an OLED display over the traditional liquid crystal displays (LCDs) is that OLEDs do not require a backlight to function. This means that they draw far less power and, when powered from a battery, can operate longer on the same charge. It is also known that OLED based display devices can be more effectively manufactured than LCD and plasma displays [47].

6.2 Applications

6.2.1 Embedded Capacitors

Lighter, smaller, compact, cheaper, finer function and further miniaturization are the keywords of today's electronics industry. To satisfy these goals, electronic packaging technology has to play a vital role [8, 19, 42, 48–53]. Discrete passives (capacitors)

are useful in applications such as noise suppression, tuning, filtering, decoupling, bypassing, termination, and frequency determination. Passives account for a very large part of today's electronic assemblies especially for digital products such as cellular phones, camcorders, computers and defense devices [19, 48–50, 52, 53]. However, they outnumber the active integrated circuits (ICs) by several times and occupy more than 70% of the substrate in a typical electronic system with the increase of frequency. Also, current interconnect technology to accommodate surface mounted passives impose certain limits on board design, which limit the overall circuit speed. Thus discrete passives have become major barriers to the miniaturization of an electronic system especially when the ratio of capacitors to total passive components could be more than 60% [54]. Many efforts were on to increase the integration density of printed circuit boards (PCBs) as part of the general effort to miniaturize electronic equipment. Additionally, as they occupy a substantial amount of surface area on a substrate, there are limitations in the number of capacitors that can be placed around a chip [53]. Hence, an obvious strategy is to reduce the number of surface mounted passives by embedding them in the substrate or printed wire board.

Embedded passives provide increased real estate on the printed wiring board (PWB), reduced parasitic effects and conversion cost, miniaturization of interconnect distance, reduced part count and improved performance [55]. For this reason, embedded passive technology, which aims at removing passive components (capacitors, resistors, and inductors) from the PCB surface and integrating them into the bulk of the boards has attracted considerable interest [50]. System-in-a-package (SIP), a novel technology, is an assembly of several types of chips such as logic, memory, analog, and passives in a package, working as one system [56]. Embedded passives, components placed between the interconnecting substrates of a PWB, play an important role in SIP technique. Integration of the passives in packages also has the benefits of higher reliability, and improved design options. Such embedded capacitors demand materials with a high dielectric constant (especially at high frequency over MHz), a low processing temperature, a low leakage current, and a reasonable high breakdown field [49, 50, 52].

Thin film deposition and anodization have been used for manufacturing embedded capacitors [57]. But, these techniques need relatively expensive equipment and are not easily implemented into large-area MCM-L (multi chip module laminated) substrates [52]. Metal organic chemical vapor deposition (MOCVD) can also be used for fabrication of high value integral capacitors where cost may not be a critical factor. MOCVD can be employed as a low temperature dielectric deposition technique as required by the PWB multi-layer fabrication technology. This technique was implemented to deposit TiO_2 thin film dielectrics at temperatures below 180°C with higher capacitance densities [52]. Two different metal-dielectric-metal type parallel plate capacitor structures on silicon and PWB substrates were developed for relatively high frequency (45 MHz–1 GHz) and low frequency (100 Hz–1 MHz) characterization (Fig. 6.1 [52]). Copper was used as the ground and upper electrodes with a 10 nm Cr adhesion layer between the dielectric and the electrodes. Specific capacitance as high as 200 nF/cm^2 was reported at 1 MHz from devices built on silicon substrates and at 100 kHz from devices on PWB substrates.

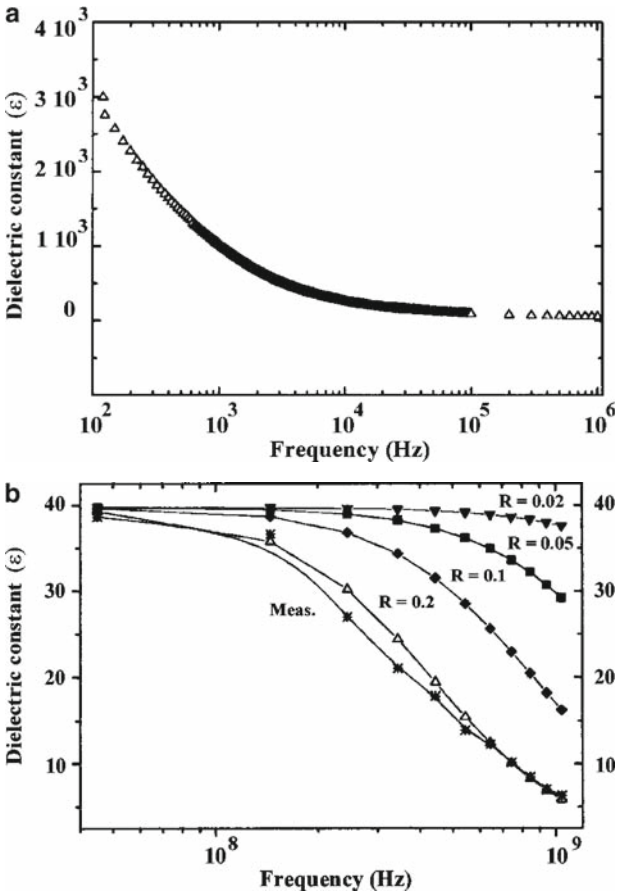

Fig. 6.1 Relative dielectric constant vs. frequency in the range (**a**) 100 Hz–1 MHz (**b**) 45 MHz–1 GHz (Reprinted with permission from [58]. Copyright (2000) Kluwer Academic Publishers)

For cost driven applications such as mobile phones and personal computers, polymer composites are the preferred materials. Polymer composite materials have emerged as a potential candidate for integral capacitors, because they satisfy the requirements of low processing temperature and reasonably high dielectric constant [53]. Many polymer nanocomposite studies focused on processing of high capacitance density thin films within small substrates/wafers where the important processing issue was to achieve high capacitance density on large coatings [54, 59, 60]. The uniqueness of polymer-based nanocomposites, compared with other nano-size objects, lies in the influence of the matrix resin on composites' performance and matrix-nanoparticle interaction. Another distinctive feature of these systems is the cooperative behavior of interacting particles in the case of highly filled composites, which becomes observable at the so-called percolation threshold where certain continuous structures of fillers are formed [61]. Novel integral passive component

materials with extraordinarily high dielectric constants ($K > 1{,}000$) and high reliability performances were demonstrated by Yang and Wong (Patented in 2001). These materials (although needed precision filler concentration control) were characterized by high dielectric constant based on the mechanism of interfacial polarization [53].

Two types of fillers have been investigated in polymers to suit as embedded capacitors: ferroelectric ceramic fillers and conducting (metallic) fillers. Properties of polymer/ferroelectric composites have been widely investigated for capacitor integration [8, 54, 59]. The dielectric constant of these composites was reported to be in the range of 10–100, depending on the ferroelectric filler concentration [62]. Also, in some cases, a high dielectric constant above 100 was reported; for example, epoxy/ceramic composites [58, 63]. Epoxy is a suitable polymer for the ceramic/polymer composites, because of its inertness to electroless plating solution and the compatibility with PWBs. Barium titanate ($BaTiO_3$) is a well-known ferroelectric material, and has a high dielectric constant around 6,000 at a fine grain size of ~1 μm, and of 1,500–2,000 at a coarse grain size [64]. Despite this, the micrometer range ceramic particles used in polymer matrix composites form weak interfaces between ceramic particles and the polymer, where more pores would form and hence lower the dielectric permittivity [65–67].

To overcome these problems, additives with high dielectric constant were used, surface modification of ceramic particles was done to improve their dispersion in the matrix, curing temperature of polymer matrix was lowered, and dielectric constant of the polymer matrix was increased [51]. Also chemical additives or shifters have been applied to the dielectric ceramics to move the Curie peak value (towards room temperature) and to smooth the Curie peak to improve the capacitance, and to have lower temperature coefficient of capacitance respectively. However these isovalent and aliovalent shifters can either decrease or increase the Curie point and change the dielectric constant. In case of modified $BaTiO_3$ high dielectric constants have been reported [64]. It is also reported that dielectric properties and the behavior of $BaTiO_3$ ceramics are highly dependent upon the particle size, grain size, phase contents, and the types of dopants added. Removal of grain boundaries, elimination of constrained forces from neighboring grains and a drop in domain density with the decreased particle size reduced the dielectric constant of the $BaTiO_3$ powders [64].

Further, conventionally to achieve high dielectric constant, the ceramic particle loading in the polymer-ceramic composite is increased. However, a high ceramic loading may lead to poor processability, poor dispersion, and therefore poor adhesion of the composite due to large loose aggregates, which in turn will effect the reliability of embedded capacitors [51]. Bai et al. [68] reported that the polymer–matrix composite with a high dielectric constant of 250 with a 50% (volume) concentration of relaxor ferroelectric ceramic particles, lost its flexibility. It was reported that a ceramic loading of above 80 vol% is impracticable. Table 6.2 lists the dielectric properties of commercial polymer-ceramic composites developed world-wide [51, 71]. Commercially available composites have only a dielectric constant of less than 40, which is far lower from the requirements for the next generation electronics. Hence, novel polymer-ceramic composites approaching the highest margin of

Table 6.2 Different commercial organic/inorganic composite materials with high dielectric constant [69, 70]

	Hadoco	3M	Dupont	Vantico
Trade name	EmCap	C-Ply	Hi-K	CFP
Composite	Epoxy/Ceramic	Epoxy/BTO	Polyimide/BTO	Epoxy/Ceramic
Thickness (μm)	100	4–25	25	12
Capacitance (pF/mm^2)	3.3	15.5–16.5	2.3	16
Dielectric constant @ 1 GHz	36	22	11.6	20.5
Dielectric loss @1 GHz	0.06	0.10	0.01	–

ceramic loading based on new concepts are needed for embedded capacitor applications. But, as per the 1998 National Electronics Manufacturing Technology Roadmap [72], a required capacitance density of ~50 nF/cm^2 by 2001 is needed for successful implementation of integral passive technology, polymer/ceramic nanocomposites proved to be a viable option for values only up to 20 nF/cm^2 [73]. Since, for higher values these nanocomposites have not been proven to be a viable solution for integration with the printed wiring boards, alternative material systems were evaluated for the critical needs as evident in the NEMI Roadmap [72].

Metal nanoparticles exhibit unique physical, chemical, optical, magnetic, and electrical properties. Many researchers have exploited their properties in a readily usable form by incorporating them into polymers [53]. The solution for the capacitors consists in embedding those components in the form of metal/insulator/metal (MIM) stacks in between the inner interconnection lines of multilayer PCBs. The advantages of this technology include increased integration density, improved reliability (reduction of solder bumps) and better electrical performances (capacitors can be located closer to active circuits) [50]. Wong et al. demonstrated metal/epoxy composites [74] for embedded capacitor applications. They fabricated epoxy/silver flakes composites with a dielectric constant of more than 1,000 which is ten times higher than ferroelectric/epoxy composites [74]. This approach is based on the fact that in metal/insulator composites, the dielectric constant is predicted to diverge at the percolation threshold [75, 76]. Li et al. [51] evaluated nickel (400 and 150 nm)-filled nanocomposite as a candidate for embedded capacitors. They reported that with highly dispersed filler even at loadings of 60 vol%, a high dielectric constant of over 90 was achieved. The change in the dielectric constant with volume ratio of the filler is demonstrated in Fig. 6.2 [51]. When the surface modification of a barium titanate (Phthalocyanine coated BTO) particle was attempted in nanocomposite, its dielectric constant was observed to be over 80 at 1 MHz, which was much higher than that of composite derived from commercial BTO. Further, to improve the processability of the nanocomposite, 4, 4′-diphenylmethane bismaleimide (BMI) was selected as a matrix polymer by the combination with polyamide (PA). Higher dielectric constant nanocomposite derived from PA/BMI and Pc-coat BTO was obtained, and its potential application towards embedded capacitors was also evaluated.

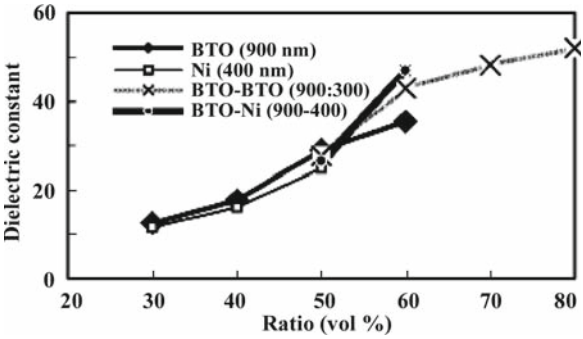

Fig. 6.2 Relationship between dielectric constant and filler volume ratio (Reprinted with permission from [69]. Copyright (2005) IEEE)

Pothukuchi et al. [53] used an in situ reduction approach to incorporate silver particles in epoxy matrix for possible use in embedded capacitor applications. Reduction of metal salt was carried out in an epoxy matrix using a reducing agent. $BaTiO_3$-epoxy based polymer nanocomposites having the potential to surpass conventional composites to produce high capacitance density, low loss, and applicable over large surface areas, in thin film capacitors were reported by Das et al. [49]. The effects of particle size, thickness and loading parameters on the observed electrical performance and the reliability of the embedded capacitors were shown. Electrical properties of nanocomposites made of epoxy (used in majority of the PCBs) resin filled with 70 nm silver particles were investigated by Gonon et al. [50] ac conductivity and dielectric constant were plotted (Fig. 6.3 [50]) in the 10^{-1}–10^5 Hz range frequency for different concentrations of silver nanoparticles. The composites exhibited electrical properties that do not obey standard percolation laws. A very low percolation threshold obtained ($\Phi c = 1\%$) was related to a segregated distribution of the fillers in the epoxy matrix. Also, they reported a very high dc critical exponent ($t = 5$), which was attributed to the inter particle electrical contact. Pecharroman et al. [78] have reported $Ni/BaTiO_3$ metal/ceramic composites with high dielectric constant of 80,000, but the metal/ceramic composites still need to be sintered at high temperature of about 1,300°C under the special protection of preventing from oxidation of Ni. Dang et al. [79] reported a three phase ($Ni/BaTiO_3$/PVDF) composite based on the mixture rules and percolation theory, with dielectric constant of above 500. These composites were prepared by simple blending and hot molding procedures and they are reported to be flexible.

Conventionally, according to percolation theories, the dielectric constant takes very large values for filler concentrations close to the percolation threshold [80–82]. So, in principle, provided one stays on the "insulating side" (filler concentrations below the percolation threshold) it is possible to get a very high dielectric constant while keeping insulating properties. Though it appears appealing, in practice this approach is not so simple to implement. Indeed, there were many examples of conductor/insulator composites for which divergence of the permittivity is not observed at the percolation threshold. For instance, in carbon black/polymer composites it was observed that the dielectric constant *smoothly* increases through

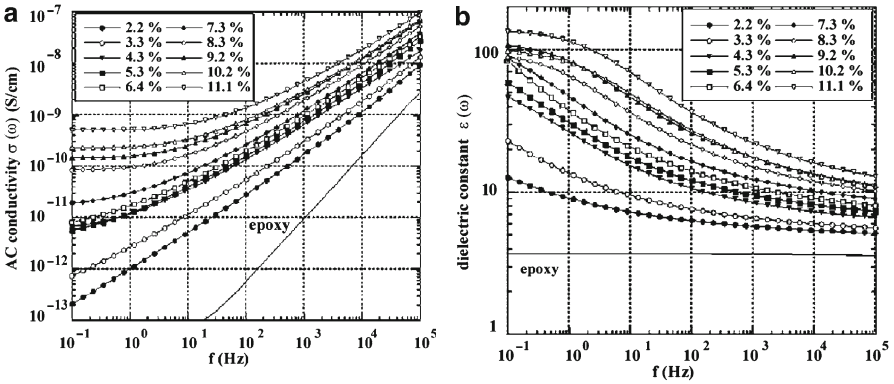

Fig. 6.3 (**a**) ac conductivity and (**b**) dielectric constant vs. frequency for various silver nanoparticles volume fraction (Reprinted with permission from [77]. Copyright (2006) AIP)

the percolation threshold (no sharp increase is observed at the percolation threshold) [83, 84]. The practical consequence is that it is not possible to get a high dielectric constant while maintaining insulating characteristics.

In a more fundamental context, conductor/insulator mixtures of several kinds were extensively studied to understand the insulator conductor transition in percolative networks [75, 76]. Concerning a segregated particle network it has been proposed that for spherical particles the following relationship should hold [85]:

$$\frac{\varphi_c}{100-\varphi_c} = 2.99\frac{D_n}{D_p},$$

where φ_c is the percolation threshold in vol% and $D_p$and $D_n$are the diameters of the polymer and the nanoparticle respectively. In a very recent work Luechinger et al. [86] studied electrical conductivity of C/Co-PEO and C/Co-PMMA nanocomposites whereby a very low percolation threshold of 0.81 vol% C/Co could be obtained. This low threshold resulted from a segregated C/Co-network located at the polymer-polymer interfaces which was corroborated by SEM-micrographs and a theoretical model. Despite numerous studies, metal/insulator composites are still motivating basic studies because deviations from standard percolation theories have been observed in many systems and some of them remain largely unexplained (as cited above, one of the "anomalous" behaviors observed in metal/insulator mixtures is the absence of permittivity divergence at the percolation threshold). A recent paper of McLachlan and Chiteme gives a good summary of such singular systems and the questions they raise about percolation theories [69].

To obtain thinner high-dielectric permittivity ceramic/polymer composite films, it is necessary to study nanocomposites that could endure the repeated changes of the heating-cooling processes when the films serve as dielectric in multilayer embedded micro-capacitors. As dielectric materials, dielectric permittivity should

increase as high as possible. But in a few cases [58, 87] results showed that the dielectric permittivity of polymer-matrix composite with micrometer-sized ceramic particles was a little higher than that with nanosized particles. This was because, tetragonality of the micrometer-sized particle is better than that of the nanosized one. Nevertheless, the thermal stability and mechanical properties of the composites will be improved when the inorganic nano-filler replaces the micro-filler in the polymer composites. Also, frequently, nanoparticles impart some particular properties to the composite only when the particles are homogenously dispersed in the polymer matrix. The polymer composites with electro-active ceramic nanoparticles were prepared using ball-milling and a sol–gel process [58, 87, 88]. $BaTiO_3$/polyvinylidene fluoride (BT/PVDF) nanocomposites were prepared via a natural adsorption action, which occurred between the nano-sized BT and PVDF particles [48]. The BT/PVDF nanocomposites without obvious BT agglomerations provided the hope of the application of the BT/PVDF nanocomposites as an alternative dielectric to embedded micro-capacitors as a result of this simple and convenient technology. Figure 6.4 [48] shows the dependence of the dielectric permittivity and loss of the BT/PVDF nanocomposites on the volume fraction of nanosized BT at different frequencies at room temperature.

Despite the positive effects of embedded nanocomposite capacitors, there is a critical issue that needs to be considered in-depth: "yield" in the manufacturing process, since embedded passive technology does not offer the luxury of reworkability, as in the case of discretes. A single defect could result in discarding the entire board with hundreds of pre-fabricated components.

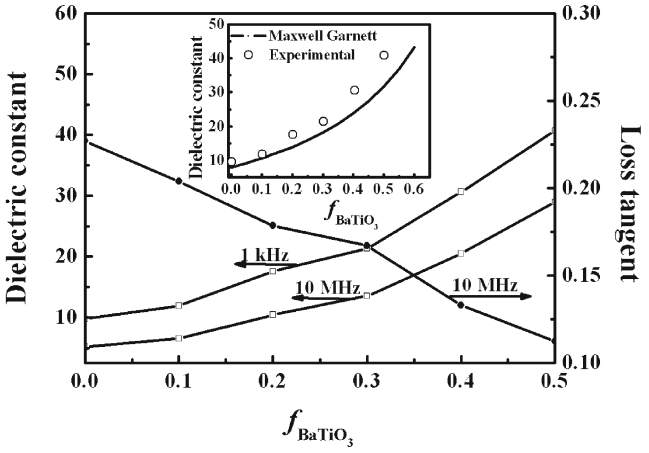

Fig. 6.4 Dependence of dielectric permittivity (*left*) and loss (*right*) of the BT/PVDF nanocomposite on the volume fraction of nanosized BT at different frequencies at room temperature. The inset is a comparison of the experimental value in dielectric permittivity to the calculated results using the Maxwell-Garnett approximation. (Reprinted with permission from [80]. Copyright (2005) Wiley VCH)

6.2.2 Lithium Ion Batteries

The improvement of preparation technology and electrochemical performance of electrode materials is a major focus of research and development in today's world. Particularly, the large scale demand for lithium rechargeable batteries or secondary batteries in day-to-day electronics (cellular phones, laptop computers, camcorders, and so forth) provided the thrust to improve their energy density, cycle life, and safety. Lithium rechargeable batteries have higher voltage (nominal voltage for Lithium ion battery is 3.6 V), higher energy density or specific energy (125 W h/kg L), and longer cycle life (>1,000 cycles) compared to conventional batteries, such as lead-acid, [89, 90] Ni–Cd, Ni–MH, [91, 92] and Ag–Zn. The performance characteristics of secondary batteries are listed in Table 6.3 [93]. Also, large-scale Li-ion batteries have great potential for electric vehicles and stationary energy storage systems.

The performances of Li-ion batteries are mainly influenced by the specific capacity and quality of the anode and cathode. During charge and discharge processes, Li ions from cathode intercalate into the crystal structure of anode and then the ions reverse direction, leaving the anode, and re-entering the cathode structure, respectively [94–96]. To achieve high cycling efficiency and long cycle life, the movement of Li ions in anode and cathode systems should not change or damage the crystal structure. Hence the physical, structural, and electrochemical properties of the cathode materials are critical to the performance of the whole battery as they provide the lithium ion source for the intercalation reaction. Figure 6.5 [98] shows a graphical representation of the energy storage capability of common types of secondary batteries.

Metallic lithium with excellent energy density was used in earlier batteries as an anodic material despite its high reactivity, which resulted in severe safety problems. For example, the dendrites grown while electroplating of Li onto the anode during charging reach the cathode resulting in an internal short, thereby leading to combustion of the Li. To overcome the problems of metallic lithium, a number of approaches/efforts were made. Scrosati et al. reported replacing metallic Li anode in Li secondary batteries with Li-insertion type of anodes [99]. Use of carbonaceous materials like graphite and artificial carbon having a graphite structure as anode materials for commercial lithium-ion batteries was also reported [100, 101]. However, the capacity of

Table 6.3 Comparison of the performance characteristics of some secondary batteries [38].

Battery	Nominal voltage (V)	Specific energy		Volumetric energy	
		(W h/kg)	(kJ/kg)	(W h/l)	(kJ/l)
Pb-acid	2	35	126	70	252
Ni–Cd	1.2	40	144	100	360
Ni–MH	1.2	90	324	245	882
Ag–Zn	1.5	110	396	220	792
Li-Ion	3.6	125	450	440	1584
Li-SPE	3.1	400	1,440	800	2,880

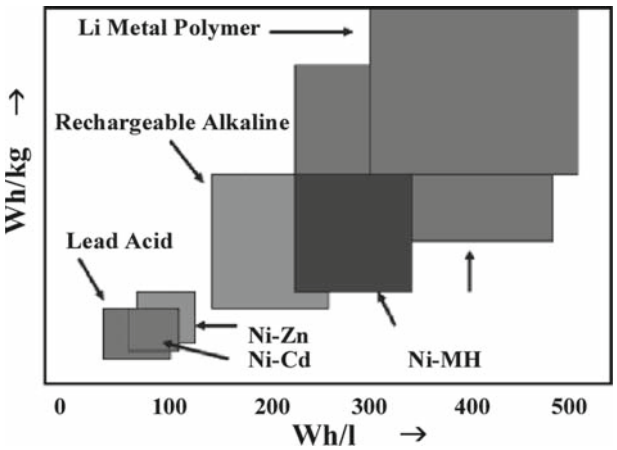

Fig. 6.5 Energy storage capability of common rechargeable batteries (Reprinted with permission from [97]. Copyright (2004) American Chemical Society)

graphite (372 mAh/g) was limited compared to that of lithium metal (3,860 mAh/g) [102]; but on the positive side, this has opened up new avenues for the deployment of transition metal oxides [103–105], metal–metal alloys [106–108], transition metal vanadates [109], ATCO anodes [77, 110], metalloids, lithium metal oxides [111], such as $LiMSnO_4$ [112], phosphates [113], niobates [114], and spinel-type ferrite anodes, viz. $CoFe_2O_4$ [115], $NiFe_2O_4$ [116, 117], $ZnFe_2O_4$ [118], and $CaFe_2O_4$ [119] for their high specific capacities and facile synthesis.

The introduction of Stalion lithium ion cells by Fuji Photo Film Celltec [95, 120, 121] whose anodes consisted of amorphous tin-based oxides instead of carbonaceous-based materials also laid the foot steps to a new generation of Li ion rechargeable batteries in the early 1990s. Materials such as SnO_2, SnO and tin glass were shown to have twice the theoretical gravimetric capacity and four times more theoretical volumetric capacity as anode active materials than carbonaceous materials [122–126]. This led to the investigation of new materials that are capable of alloying with lithium such as Al, Sn, Pb, In, Bi, Cd, Ag, Mg, Zn, Si, and Sb [123, 124, 127]. These materials though showed satisfactory Li-ion transport properties, good lithium packing density and electrochemical potential, a substantial change in specific volume of the electrode upon continuous cycling resulted in loss of electrical contact, and thus capacity loss as well as macroscopic dimensional problems within the cell structure. For example, a large irreversible capacity loss at the first cycle due to a reduction reaction [127] prevented tin oxide anode materials from having any practical application. According to previous reports, tin oxides are reduced during the first discharge to form fine particles of tin and inactive phases like Li_2O, which slowed the growth of tin [123] leading to an excessive usage of cathode materials. Also, large tin oxide particles pulverize rapidly during discharge and charge cycles due to volume mismatch, resulting in a rapid drop in reversible capacity upon cycling.

In case of small particles, because the nanometer sized cavities within powders absorb the expansion of materials during the formation of lithium compounds, pulverization was thought to be less extensive. Silicon has the highest theoretical capacity of 4,000 mAh/g when forming $Li_{4.2}Si$ alloys. However, this alloying process is associated with a 300% volume dilatation, pulverizing the brittle electrode and inducing poor cyclability [6]. Limitation of cycling depth with a very thin reaction layer [128, 129], reducing the metal particle size [95, 130], or construction of bonded electrodes using Li^+-conducting intermetallic phases [6, 131] were among the several methods proposed to solve the problem of volume expansion. It was thus postulated that nanostructured or amorphous electrodes may reduce the extent of pulverization, and thereby improve the cycle life of the electrode [132, 133].

Since many nanomaterials show higher reversible capacity than the corresponding micro-sized materials for anodes of lithium ion batteries, they have attracted great interest for lithium secondary batteries [134–138]. Carbon nanotubes [139–143], intermetallics, nanocomposites [98, 144], nano-oxides [104, 144–146], nanocrystalline thin films [147] are some examples, which have been reportedly used as anode materials to improve lithium storage capacities. Among these, single walled carbon nanotubes (SWNTs) showed a reversible capacity of 600 mAh/g [143]; a nanocomposite of Si [148] exhibited better cycling performance and reversible capacity of over 1,700 mAh/g at room temperature; and nano-sized transition-metal oxides delivered a Li storage capacity of ~700 mAh/g with 100% capacity retention for up to 100 cycles [104]. Chen et al. [45] reported the usage of nanocomposites of carbon nanotubes with Sn_2Sb alloy nanoparticles as anode material for Li ion batteries and showed that the first cycle de-lithiation capacity of 580 mAh/g from a carbon nanotube-56 wt% Sn_2Sb nanocomposite was reduced to 372 mAh/g after 80 cycles. Moreover, Sony commercialized [149] the first tin-based anode battery in February 2005, and Toshiba Corporation in March 2005 announced [149] a breakthrough technology using nanoparticles as negative electrode of Li-ion batteries.

Further, Li et al. [134, 135] reported high capacity and good cyclability for nanostructured tin oxides prepared by templating technique. Likewise, Yang et al. [133, 138] found that ultra-fine Sn-SnSb particles with $d_p < 300$ nm substantially raise the electrochemical performance of tin based alloys. The authors have attributed the improvement to the stabilization of the nano-sized alloy particles against agglomeration during Li insertion and extraction reactions. Carbon nanotubes were also used as one-dimensional hosts for the intercalation of Li and other alkali metals. It was demonstrated that multi-walled carbon nanotubes (MWNTs) could accommodate very high Li concentrations if insertion was carried out in the molten state at high pressures [150]. Reversible capacities were found to be in the range of 80–640 mAh/g for carbon nanotubes, in general, and further increase after ball milling. For example, Chen et al. reported the reversible capacities for single-walled nanotube electrodes after ball milling from 600 to 1,000 mAh/g [141, 151, 152]. However, a large voltage hysteresis in the first electrochemical extraction reaction of Li^+ was observed in all studies, in turn dampening the interest in using nanotubes as a viable Li-ion storage compound.

In addition, aggregation of nanotubes during cycling is a major challenging problem, which gives rise to poor cycling performance and thus limiting their practical applicability. Many efforts were put-forth to disperse the nanoparticles homogeneously in a matrix [153] and also to synthesize metal-encapsulated spherical hollow carbon [154], in order to improve their cycling behavior. But, none of these methods resulted in significant progress. A few studies were also focused at the usage of nanocomposites as anode materials in Li-ion batteries [6, 45, 95–98, 100, 102, 131, 155–157]. 10.3 wt% 3.5 nm Sn-graphite nanocomposite made from an in situ formed $SnCl_4$ precursor displayed a high reversible Li^+ storage capacity of 415 mAh/g, of which 91.3% was retained after 60 charge and discharge cycles, and demonstrated that particle size and distribution are both very important factors determining the applicability of Sn-based nanoparticles in Li-ion batteries [158].

It is always highly desirable to apply simple and highly productive techniques to produce both the anode and cathode materials despite the various methods available for the production of the ultrafine nanoparticles used in Li-ion batteries. Spray pyrolysis, an in situ fabrication technique, is one such method because it is inexpensive, versatile, industrially oriented, and can be operated over a large temperature range (100–1,000°C) [128, 129, 159, 160]. Martos et al. [129, 159] used sprayed lead oxide powders as anode material in Li-ion batteries and showed that the specific capacity fades on cycling when bulk powders were used. Recently, Ng et al. [95] have suggested the addition of a carbon source (sucrose solution) to enhance the electric conductivity of PbO [160–162]. The combination of spray technology and carbon addition increased the specific surface area (above 6 m^2/g and the conductivity of PbO, improved the specific capacity, and maintained a cycle life with a reversible capacity above 100 mAh/g beyond 50 cycles) [95]. The increase in capacity retention for PbO–carbon compared to pure PbO was attributed to the presence of a conductive and highly developed carbon matrix (an excellent electric conductor) that can absorb large volume changes during alloying/dealloying of lead with [163, 164] lithium over the 1.50–0.01 V potential range. Also, with increasing carbon content, an improved cycle life of the PbO–carbon nanocomposites was reported (Fig. 6.6 [95]).

Different from the traditional methods (polymer coating, self assembly and layer by layer formation [136]) to synthesize core/shell nanocomposites, Fu et al. employed emulsion polymerization method followed by heat treatment to synthesize the core/shell structured TiO_2/C nanocomposites [155, 165]. These nanocomposites proved to be a good way of improving the cycling behavior and kinetics of lithium intercalation and de-intercalation of nano-titanium oxides [156]. They have shown that the thickness of carbon shell and the number of TiO_2 nanoparticles in the shell can also be controlled. In Fig. 6.7, [156] the discharge and charge curves of virgin TiO_2 and TiO_2/C nanocomposite electrodes are shown. The charge capacity of TiO_2/C nanocomposite remained at 96.7% (i.e., 118 $mAhg^{-1}$ titania) of its original capacity (i.e., 122 mAh/g titania) even after 10 cycles, which was much higher than that of virgin TiO_2 nanoparticles whose anode retained only 67.5% of the original capacity. This was thought to be due to the suppression of the aggregation

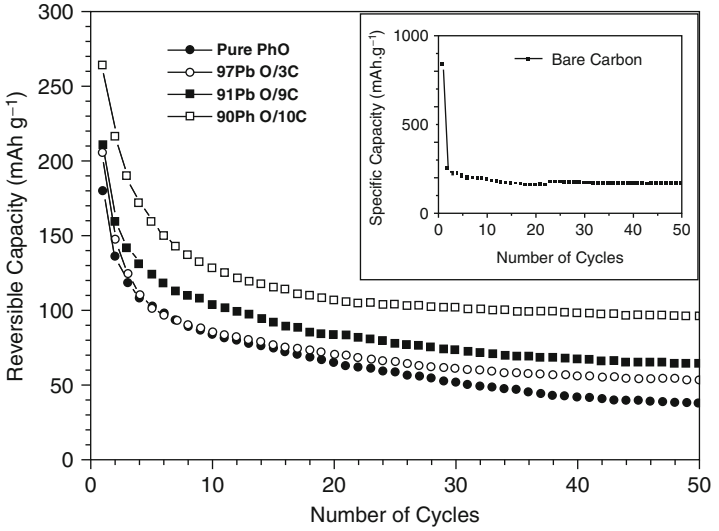

Fig. 6.6 Cycle life of PbO–C nanocomposites. The current density was 0.100 mA/cm^2. The inset figure presents the specific capacity vs. cycle number data for the bare carbon powder and the current density applied was also 0.100 mA/cm^2 (Reprinted with permission from [40]. Copyright (2006) Electrochemical Society)

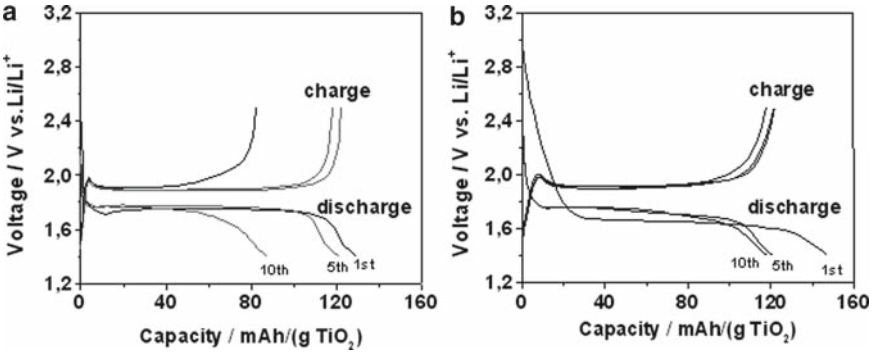

Fig. 6.7 Discharge and charge profiles of: (**a**) the virginal TiO_2 nanoparticles and (**b**) the TiO_2/C core–shell nanocomposite at a constant current density of 0.1 mA/cm^2 (0.25 C) in the voltage range 1.4–2.5 V (Reprinted with permission from [37]. Copyright (2006) Elsevier)

of nanoparticles by the coated carbon shell. They also reported that the nanocomposites exhibited higher apparent diffusion coefficients of lithium ions compared with virgin TiO_2 nanoparticles.

For the first time, Selvan et al. [96] have reported the use of $CuFe_2O_4/SnO_2$ nanocomposites (synthesized by means of a urea–nitrate combustion method) as anode materials for Li-ion batteries. They showed that the electrochemical activity of native $CuFe_2O_4$ was enhanced through the incorporation of SnO_2 and also identified

the advantages of deployment of nanocomposite electrodes and the effect of SnO_2 dopant in reducing the Li+ ion diffusion path lengths so as to enhance the diffusion kinetics and impart improved charge–discharge characteristics. The coulombic efficiency of copper ferrite anodes is improved from 65 to 99.5% through SnO_2 doping. Figure 6.8 [96] represents the charge-discharge profiles exhibited by $CuFe_2O_4$ and $CuFe_2O_4/SnO_2$ anodes. The high specific capacity values exhibited by both the ferrite anodes (>800 mAhg [20] were attributed to the electrochemically driven size confinement of the nano electrodes.

The nano $CuFe_2O_4$ anode and $CuFe_2O_4/SnO_2$ nanocomposites delivered an improved specific capacity of 1,193 and 849 $mAhg^{-1}$, respectively, which were almost three times higher than that of a carbon anode (372 mAh/g). Ahn et al. [102] also have investigated the effect of dispersion of alumina particles on the electrochemical properties of Sn, SnO_2, and tin based intermetallic Ni–Sn as anode materials for Li-ion batteries. They have synthesized various tin-based nanocomposite anodes with Al_2O_3, using high-energy ball milling. The first charge (Li-insertion) capacities were found to be very high for these composite electrodes. However the nanosize oxide dispersion did not improve cycle properties of tin-based anodes.

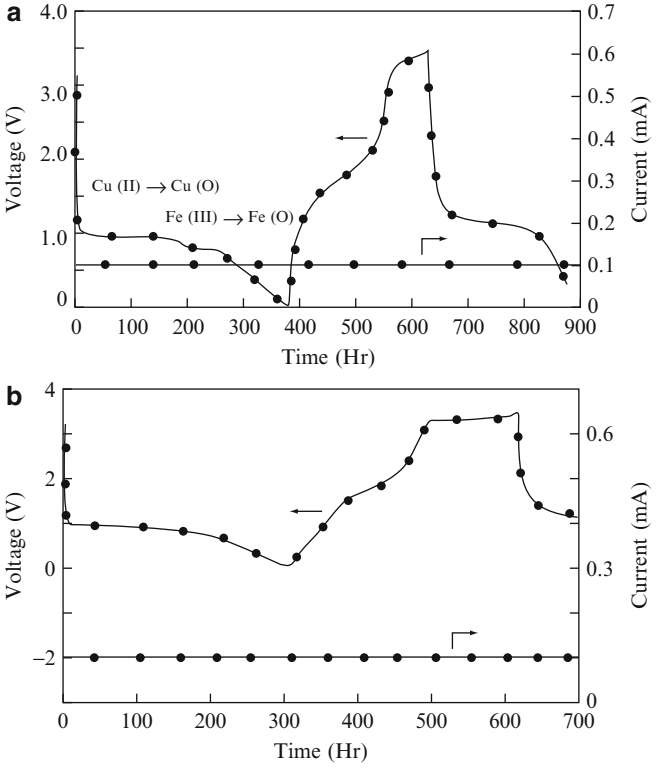

Fig. 6.8 Charge–discharge profiles exhibited by (**a**) $CuFe_2O_4$ and (**b**) $CuFe_2O4/SnO_2$ anodes (Reprinted with permission from [131]. Copyright (2006) Elsevier)

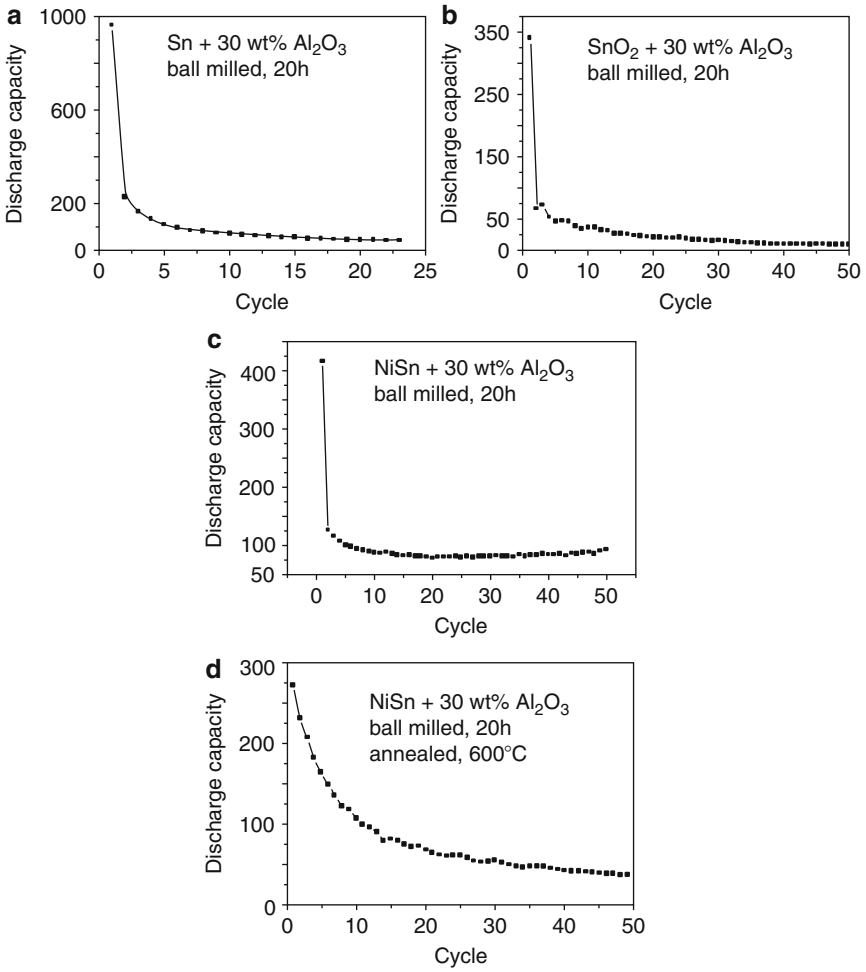

Fig. 6.9 Change in charge capacities on cycling for different nanocomposites (Reprinted with permission from [22]. Copyright (2003) Elsevier)

Figure 6.9 [102] shows the change in charge capacities for different nanocomposites on cycling.

Furthermore, nano-dispersed Si in carbon synthesized by chemical vapor deposition (CVD) had demonstrated a reversible capacity of 500 $mAhg^{-1}$. However, the CVD approach produced SiC and the morphology of Si and C cannot be controlled [166]. Nanostructured thin-film form of Si electrode was investigated by some researchers and they reported a specific capacity of around of 1,100 mAh/g [167, 168]. Nano Si–C composite prepared by hand mixing has been reported to have a high reversible capacity of 1,700 mAh/g by Li et al. [148]. Also crystalline Si powders have been dispersed in sol–gel graphite [169], in a TiN matrix [153], and in synthetic graphite [170], by ball milling. All the Si–C composites mentioned, exhibited increased specific capacity

compared to bare graphite, and improved cyclability compared to bare Si electrodes. Wang et al. [157] have reported the synthesis of nanostructured Si–C composites by dispersing nanocrystalline Si in carbon aerogel. A reversible capacity of 1,450 $mAhg^{-1}$ for Si–C composite electrodes (Fig. 6.10a [157]) was reported. The good cyclability was attributed to the usage of nano-sized Si powders and their homogeneous distribution (Fig. 6.10b [157]) in an amorphous carbon matrix.

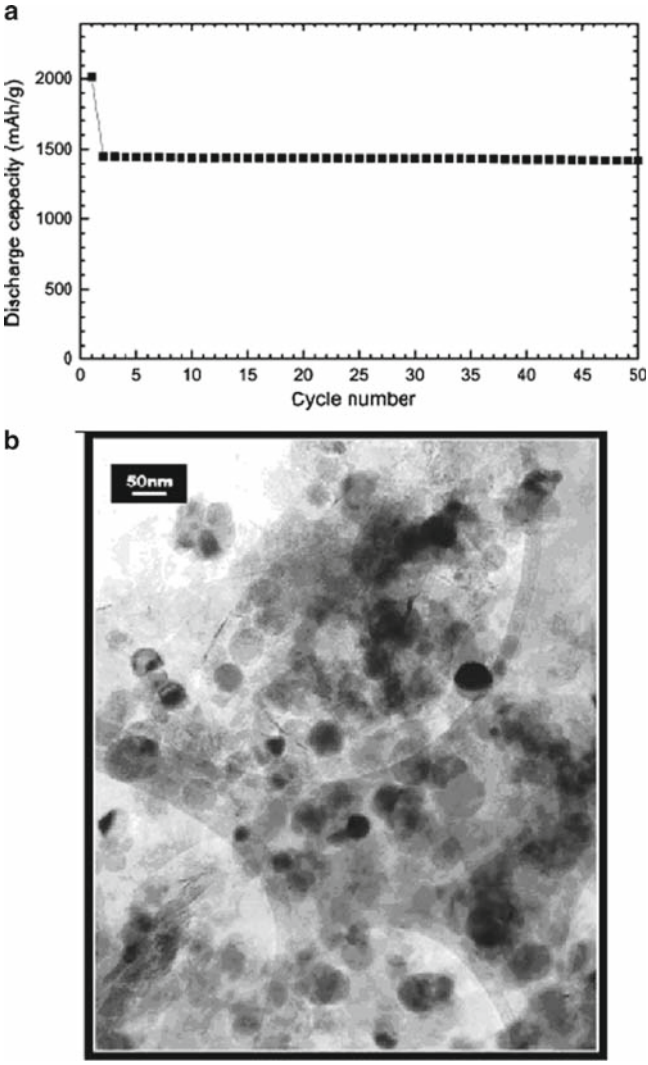

Fig. 6.10 (**a**) The discharge capacity vs. cycle number for Si–C electrode. (**b**) TEM image of nanocrystalline Si–C composites (Reprinted with permission from [171]. Copyright (2004) Elsevier)

A challenge in working with nanocomposites and nanostructured materials derives from difficulties in obtaining adequate structural characterization, especially, as they often lack long-range order. For example, although XRD can yield valuable information regarding structural changes that occur in the host material during Li^+ insertion, the poor crystallinity of organic–inorganic hybrid nanocomposites limits the applicability of this technique. So the results obtained exclusively from this technique should be addressed in terms of their accuracy. Nuclear magnetic resonance technique is proved to be a better alternative for this purpose.

6.2.3 Integrated Circuits

Meso-, micro-, and nano-porous materials are of much interest in the microelectronics industry due to their potential use as low dielectric constant (low-*k*) interdielectrics [35, 122, 172–174], in integrated circuits (ICs) with multilayer structures. They can lower line-to-line noise in interconnects and alleviate power dissipation issues by reducing the capacitance between the interconnect conductor lines. In addition to providing device speed improvements, low-*k* interdielectrics also provide lower resistance-capacitance delay, making them superior to low resistivity metal conductors such as copper and silver [33, 173, 175]. Thus, interdielectric materials with $k \ll 2.5$ are in high demand in the microelectronics industry, which is rapidly developing advanced ICs with multilayer structures that have improved functionality and speed in a smaller package and also consume less power [33, 173, 175].

As per "The Semiconductor Industry Association's International Technology Roadmap" for semiconductor materials, materials with an effective *k* of 2.5–3.0 are in production today, and that in the near future, material systems that deliver an effective $k < 1.9$ are expected to be available, in particular for 50 nm or less feature size technology based on copper metallization [175]. However low-*k* dielectric materials must meet the thermal stability requirements of the metallization processing of ICs. For example, low-*k* nanoporous materials should withstand high temperatures during the processes like copper metallization, which are conducted at <250°C; and generally, are followed by thermal annealing in the range 400–450°C to ensure the production of void-free copper deposits. Moreover, these materials also have to meet conditions such as [35, 176]: low moisture uptake, high purity, good adhesion to silicon, silicon oxide and metals, good planarization behavior, and appropriate plasma etching behavior. Interdielectric materials also have to be able to withstand harsh chemical mechanical polishing (CMP) conducted with an aqueous slurry containing an abrasive (e.g., alumina particles) and an oxidant and/or complexing agent (e.g., nitric acid or ammonium hydroxide) to remove excess metal during the metal inlay process [35, 176].

A wide variety of polymers have been reported as potential low-k materials for use in the development of advanced ICs such as polyimides, heteroaromatic polymers, polyaryl ethers, fluoropolymers, non-polar hydrocarbon polymers, and polysilsesquioxanes [34, 164, 177, 178]. The dielectric films of these materials can be deposited from the gas phase with chemical deposition, plasma enhanced chemical vapor deposition, and other techniques. Polytetrafluoroethylene has a k value of 2.2, the lowest reported so far for such polymers. However, its very poor mechanical properties, poor interfacial adhesion and poor processability out-list PTFE for use in the fabrication of ICs. Nevertheless, the k value of these polymers ($k \sim 2.5$) is lower than those of today's workhorse dielectrics silicon dioxide ($k = 3.9$–4.3) and silicon nitride ($k = 6.0$–7.0), and still much higher than that of air (or vacuum), $k = 1.01$, which is possibly the lowest value attainable. So, the idea of incorporating air into dielectric materials as nano-pores to produce nanoporous materials with low k values has attained much interest [33, 173, 174]. To prevent the metal diffusion into the interdielectric layers during the IC fabrication, the nano-pores have to be at least 5–10 times smaller than the minimum IC metal feature size.

The dielectric constant obtained is limited primarily due to the intrinsic dielectric constant of the matrix and the sizes of the dispersion pores in the materials. The ultimate aim of the introduction of nanometer-sized pores into these materials is to increase the amount of free space. Matrices containing homogeneous, nanometer-scaled, and closed pores were preferred in terms of their electrical and mechanical properties and the effect porosity on dielectric constant can be predicted using simple models, such as the Bruggeman effective medium approximation [34]:

$$f_1 \frac{k_1 + k_e}{k_1 + 2k_e} + f_2 \frac{k_2 - k_e}{k_2 + 2k_e} = 0$$

where, f_1 and f_2 represent the fractions of the two components, $k_1$and k_2 are the dielectric constants of the components, and $k_e$is the effective dielectric constant of the material. The assumption here is that the material has two components, matrix and pores. When the porosity exceeds 30%, the pores will become percolated or interconnected causing local trapping of moisture and chemicals, which leads to an increase in dielectric constant, and crack formation.

Films of poly(*p*-phenylene biphenyltetracarboximide) containing 27 wt% hollow sphere silica nanoparticles (with refractive index of 1.7007 at a wavelength of 830 nm) were prepared by thermal sintering of monolithic silica aerogels [35]. These hollow nanoparticles were thermally stable and withstood temperatures of up to 500°C, which made them useful for incorporation in organic polymers such as polyamide, other high temperature polymer dielectrics and inorganic dielectrics such as silicates and organosilicates. However the size of these nanoparticles (150 nm) was larger than the actual metal features of the advanced ICs.

Generally, studies on porous materials were based on two routes: (a) thermal decomposition of polymer blends or by block copolymers and (b) blending of a highly thermal stable polymer [179–181] with an unstable one. Carter et al. [180] developed a highly fluorinated polyimide with low dielectric constant of $k < 2.3$ by

Table 6.4 Dielectric constant of polyamide nanoporous materials [29]

	PEO–POSS in feed				
Sample	wt%	mol%	Dielectric constant (K)	Thermal expansion coefficient (ppm) 50–250 (°C)	Measured density (g/cc)
PI-0P	0	0	3.25	38.2	1.38
PI-2P	2	0.0007	2.88	42.3	1.31
PI-5P	5	0.0017	2.43	46.5	1.18
PI-10P	10	0.0034	2.25	55.8	1.09

using the nano-foam approach. However, fluorinated polymers have inadequate thermal stability for use in integration procedures, and there are issues for fluoric acid evolution during processing and reactions with the metals used [182, 183]. Block copolymers usually consist of a highly temperature-stable block and a thermally labile block that acts as the dispersed phase through the curing process, which makes them good candidates for templates. Thermolysis of the labile blocks leaves pores of sizes and shapes that correspond to those present in the initial copolymer's morphology. A number of reports [179, 180, 182] described the synthesis of porous structures of high temperature thermoplastic materials ($Tg > 350°C$) from block copolymers. Lee et al. [184] synthesized nano-porous polyimide films through the use of a hybrid poly(ethylene oxide)–polyhedral oligosilsesquioxane (PEO-POSS) template. Reduced dielectric constant of $k = 3.25–2.25$ of the porous hybrid films with pore sizes in the range of 10–40 nm were reported. Table 6.4 [184] gives the dielectric constants of the various composites having different POSS contents.

6.2.4 Transistors

Field effect transistors (FETs) play a significant role in modern electronics as they are inherent parts of various devices, for example, computer chips. It is crucial to develop novel device geometries to optimize gate electrostatics needed for efficient ON-OFF switching for highly scaled molecular transistors with short channels [1]. Composite materials based on the coupling of conducting organic polymers (COPs) and carbon nanotubes (CNTs) offer an attractive route to introduce electronic properties [20, 185–188]. Some of the COPs used are polyaniline (PANI) [5, 189–191], polypyrrole (PPY) [192–194], polythiophene (PTh) [195], poly(3,4-ethylenedioxy thiophene) (PEDOT) [193, 194, 196], poly(*p*-phenylene vinylene) (PPV) [186], and poly(m-phenylene vinylene-co-2,5-dioctoxy-*p*-phenylene) (PmPV) [192, 197]. It was also suggested that in COP/CNT composites, either the polymer functionalizes the CNTs or the COPs are doped with CNTs, i.e., a charge transfer occurs between the two constituents [1]. Qi et al. [198] showed that SWNT-contacted P3HT FETs exhibited higher current modulation of three orders of magnitude than the metal contacted devices over a same gate voltage (−2 to 2 V gate range). However, there

are many problems associated with the use of carbon nanotubes to be overcome, if their potential towards the field of transistors has to be fully realized, which will be briefly discussed in this section.

Carbon nanotubes, particularly, single-walled carbon nanotubes (SWNTs) generated much interest as they possess unique electronic properties, high chemical stability, impressive mechanical strength and excellent thermal and electrical stability [12, 26, 27]. Their potential use in a variety of technologically important applications, such as electronic devices, field effect transistors, molecular diodes, memory elements, logic gates, molecular wires, high strength fibers, sensors, and field emission is very well established [12, 32]. Dekker [199–201], Lieber [202–204], and Avouris [205] demonstrated that SWNTs can be used as semiconducting channels in functional field effect transistors (FETs) and also outperform comparable Si-based devices [32]. Dai and co-workers showed that SWNTs can act as chemical sensors, where exposure to specific gases, including ammonia, hydrogen and NO_2 alters nanotube conductivity by up to three orders of magnitude within several seconds of exposure [32]. However, their structural resemblance to graphene, limits their flexibility for practical applications due to their high chemical stability and insolubility in most organic and aqueous solvents. This limiting factor must be overcome if carbon nanotubes are to be utilized, especially in the preparation of blends with conventional polymers, molecular electronics, and the production of homogeneously dispersed conducting layers within electroluminescent devices [12, 32].

To modify their structure, especially to improve their solubility, compatibility, chemical reactivity, and electronic properties [12] generally, CNTs are functionalized with various organic, inorganic, and organometallic structures using both covalent and non-covalent approaches with a primary focus of improving the solubility properties. Initial success was achieved by functionalizing carboxylic acid groups, formed at the ends and defective sites of SWNTs during oxidative purification/shortening through amidation with alkylamines such as octadecylamine [206]. Later, this approach has been extended to the attachment of organometallic complexes, including Vaska's complex [207] and Wilkinson's catalyst [208], inorganic nanocrystals such as CdSe [209] and Au, DNA, and various other biological molecules, dendrons, and polymers. Another strategy for SWNT functionalization involves the use of side-wall reactions such as fluorination with elemental fluorine, 1,3-dipolar cyclo addition, electrochemical reduction of diazonium salts, and direct addition of nitrenes, carbenes, and radicals to the unsaturated π-system of the nanotubes. The covalent functionalization strategies opened up a wide range of chemistry that can be performed on the sidewalls of carbon nanotubes, which allow chemists to control the properties of these nanoscale materials.

Functionalization with monolayer protected nanoclusters (MPCs) is highly promising and many researchers have focused on gold nanoclusters because of their special optical properties, unusual electronic properties, remarkably high catalytic activity, and so forth. MPCs are generally organized on pre-functionalized nanotube surface either by covalent, hydrophobic or hydrogen bonding. Geckeler et al. arranged gold nanoparticles on SWNTs by the addition of metal salts to surfactant-suspended SWNTs in water using the solution phase dispersion technique [12].

Recently, Mahima et al. [12] reported an electrochemical route to assemble monolayer protected gold nanoclusters (AuMPCs) on the surface of SWNT bundles, by applying an external potential. This electrochemical process for preparing hybrid nanoscale materials has added advantages compared to other chemical routes, which normally include undesirable sidewall reactions, tedious purification processes, and shortening of the tubes due to the use of strong oxidizing agents, which introduces defects on the side-walls, making them less useful for potential electronic applications. The authors reported significant enhancement in double layer capacitance (almost ten times greater) for these hybrid materials as compared to bare SWNTs.

Further, a number of recent reports have concentrated on supramolecular functionalization of SWNTs, especially with polymeric structures. Aromatic sidewalls of nanotubes provide the possibility for π-stacking interactions with conjugated polymers as well as polycyclic aromatic hydrocarbons [32]. Substituted pyrene molecules were also employed for surface attachment of a number of functionalities where the appended structure has been used to attach proteins, polymerization initiators, or aqueous solubilizing groups in a non-covalent fashion. So far, covalent attachment of polymers to carbon nanotubes has been mainly accomplished using a "grafting to" approach, in which the polymer is first prepared and then reacted with the carboxylic acid functionalities of the SWNTs.

As different from that approach, Yao et al. [32] described a "grafting from" approach to the "growth" of polymers from the surface of nanotubes by first covalently attaching polymerization initiators and then exposing the nanotube-based macroinitiators to monomers. It was believed that a higher incorporation of polymers would result relative to the "grafting to" approach because this approach strictly involves the reaction of the nanotubes with small molecules. They investigated the use of atom transfer radical polymerization (ATRP) which has been shown to be a highly versatile technique for the controlled radical polymerization of acrylate based monomers from the surface of nanoscale structures. SWNTs were functionalized along their side-walls with phenol groups using the 1,3-dipolar cyclo addition reaction and the phenols were further derivatized with 2-bromoisobutyryl bromide, resulting in the attachment of atom transfer radical polymerization initiators to the sidewalls of the nanotubes. They also reported that nanotubes functionalized with poly(methyl methacrylate) were found to be insoluble, while those functionalized with poly(tert-butyl acrylate) were soluble in a variety of organic solvents. The tert-butyl groups of these appended polymers were removed to produce nanotubes functionalized with poly(acrylic acid), resulting in structures that were soluble in aqueous solutions [32].

Due to their low carrier mobility, conducting polymer based thin film transistors suffer from inferior performance when compared to inorganic crystalline semiconductors [1, 5]. The properties of the individual molecules and structural order of the molecules are the key factors determining the macroscopic properties of the organic semiconductor materials. Large π-conjugation length, high degree of ordering, and molecular packing are important factors for carrier mobility in conducting polymers [210, 211]. Polyaniline is an outstanding conducting polymer in which the conductivity results from a process of partial oxidation. It is interesting because of its good stability

in the doped form and electronic properties. Based on morphological modification or electronic interaction between the two components, carbon nanotubes in conducting polymers were shown to possess properties of the individual components with a synergistic effect [20, 186, 194]. Carbon nanotubes will not only allow the carriers to be transported by providing percolation paths, but also help to improve the mobility. The transfer characteristics' analysis of the field effect transistors (FETs) suggested that the carbon nanotubes have a higher carrier density than graphite and a hole mobility comparable to that of heavily p-doped silicon [212].

In the core shell structure of the polyaniline (shell)/CNT (core) nanocomposites obtained by in situ polymerization, the presence of CNTs have improved the polymer properties by (a) inducing additional structural ordering of the polymer; (b) enhancing thermal stability; (c) enhancing delocalization of charges in the composite; (d) improving the compactness and conjugation or chain length; and (e) improving charge carrier mobility [8]. These properties are desired for a material in the field of organic electronics. DuPont have developed polyaniline/carbon nanotube composites as printable conductors for organic electronics applications [29]. Ramamurthy et al. [213] reported that improvement in material consistency and reduction in defect densities will make these composites suitable for use in fabricating organic electronic devices. It was suggested that by finely dispersing the carbon nanotubes in a polymerization medium, during in situ polymerization, a good level of homogeneity can be achieved further enhancing the material quality.

Kuo et al. demonstrated polyaniline without any side chains to be the active layer in an organic thin film transistor (TFT) and high field effect mobility was observed [214]. Carbon nanotube nanocomposites used for thin-film transistors provide one of the first technologically-relevant test beds for two-dimensional heterogeneous percolating systems. The characteristics of these TFTs are predicted by considering the physics of heterogeneous finite-sized networks and interfacial traps at the CNT/gate-oxide interface. TFTs based on two-dimensional networks of carbon nanotubes or silicon nanowires were recently explored for low voltage, high reliability, and high-speed applications in flexible macro-electronics [171, 215, 216] as well as in CNT microelectronics [217, 218]. A number of technical difficulties remain, despite their promise to improve the performance of micro- and macro-electronics, such as: poor sub-threshold characteristics and lack of understanding of on-off current dependence on parameters such as the channel length, tube length, and the fraction of metallic tubes. Properties of these two dimensional CNT networks are controlled by the competition between heterogeneous networks of metallic and semi-conducting CNTs, a regime that has never before been explored. A predictive model is required to interpret experimental results and to expedite the development of this new class of TFTs.

Kumar et al. [27] have developed a heterogeneous finite-size percolation model to explore the dependence of gate characteristics in the linear regime on tube density and metallic contamination for thin films made of randomly oriented nanotubes. The authors explained the on-off ratio before and after the breakdown of metallic tubes. The developed model also answered two questions of fundamental technological importance: (1) What are the performance limits of network transistors free

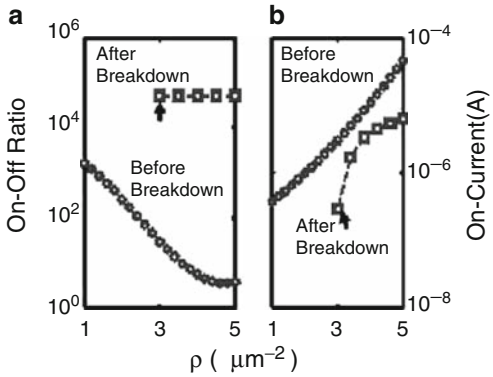

Fig. 6.11 Dependence of (**a**) On-off ratio and (**b**) On-current on network density before and after the removal of metallic tubes. L_S = 10 μm, L_C = 2 μm, and H = 35 μm. The network drops below the percolation limit after breakdown for the tube density indicated by arrows (Reprinted with permission from [7]. Copyright (2006) AIP)

from metallic tubes (f_m (metallic tube fraction) = 0)?, and (2) given a technology-specific f_m, what is the maximum density of tubes that will preserve a high on-off ratio? Figure 6.11 [27] represents the results obtained from the model for the on-off ratio before and after the break down. Close agreement between numerical results and different experimental observations was also achieved demonstrating the capability of this model to predict the characteristics of CNT/nanowire-based TFTs. Such predictive models would simplify device optimization and expedite the development of this nascent TFT technology.

Organic thin film transistors though attracted a great deal of interest (as critical components for the fabrication of low cost and large area flexible displays and sensors), the major problem in using them in the logic circuits is the requirement of high operating voltage. This problem needs to be focused in order to realize the full practical applicability of these materials.

6.2.5 Information Storage

It is evident that modern information systems, in particular, electronic systems inevitably reach the fundamental technological, physical, and functional limitations. The fact that fiber optics communications is an advanced field of business today shows that from the view-point of information carrier, photon is considered as an alternative to electron [10]. Telecommunication networks mainly develop in a so-called "third telecommunication window," i.e., in the range of silica fiber (minimum absorption near the wavelength of ~1.5 μm), and erbium doped optical fibers (generally, used for amplification of optical signals [70] to achieve high amplification with low noise [219]).

Photonic devices based on integrated optics and hybrid systems that use micro-laser and other micro- and nano-optical elements are playing a significant role. These systems demand a short effective gain length and, consequently, a higher concentration of active medium. To meet this new active media, methods that obtain high doping concentrations should be used and also concentration quenching be surmounted.

Photonic crystals (periodic quantum-dimensional systems) present a new type of artificial media possessing a spatial periodicity of optical properties with the period of the order of optical wavelength [219]. There are possibilities to control photons in such media, which are advanced in various fields of modern optics and nanophotonics. It was reported that most promising technologies for forming new media with quantum-dimensional properties are those based on self-organizing systems [219]. Photoluminescence of nanocomposites based on cubic packing SiO_2 nanospheres (opal matrices) and porous anodic alumina (PAA) doped with erbium and other rare earth elements, vs. the element structure, concentration of rare earth ions, matrix composition, optical properties, and technology was studied by Tsvetkov et al. [219]. Fig. 6.12 [219] shows the images of these materials. They also discussed the possible application of 3D-(space) and 2D-(planar) nanocomposites in systems of optical information transfer, storage, and processing.

The progress of information technology depends critically on the development of new materials for high density optical and magnetic memory storage. The last decade has seen a great research effort in the case of optical data storage, geared towards development of bit-oriented 3D, or multilayered, optical memories based on a variety of materials. 3D media promises a dramatic increase in memory capacity as the storage density scales as $1/\lambda^2$ and $1/\lambda^3$, where λ is the wavelength of the reading beam, for 2D and 3D optical memories, respectively [221]. Rentzepis et al. [222] explained the approach of bit-oriented 3D optical memory based on two-photon writing for the first time. It was shown that simultaneous absorption of two photons from overlapping laser beams led to excitation of the photochromic molecule, spirobenzopyrane, which was molecularly dispersed in a polymeric matrix. The intersection of the two laser beams at different spots in the material led to spatially resolved photochemical changes in the bulk material. The "written" state was sufficiently stable to be accessed or "read" [221].

A variety of media, have explored the use of photoinduced effects such as photochromism, photorefractivity, photobleaching, carbonization, microexplosions, photoluminescence, and photopolymerization as the basis for information storage, while a broad range of microscopy techniques have been used to read the data written in 3D space [219, 223–225]. All these research studies have considered homogeneous recording medium (storage density can be as high as 10^{12} bits/cm^3) [219, 223, 225]. In other words, it was either represented by a single-component photosensitive film material or contained low-molecular-weight photosensitive species uniformly dispersed in a film-forming matrix. Siwick et al. [10] reported the use of a hexagonally close-packed (HCP) array of fluorescent particles periodically embedded in an optically inert polymer matrix. Optical recording in the nanocomposite was accomplished by photo bleaching the fluorescent dye incorporated in the particles with a laser confocal fluorescence microscope [10]. However, they showed that their approach did not exploit the periodically modulated optical properties of the nanocomposite since

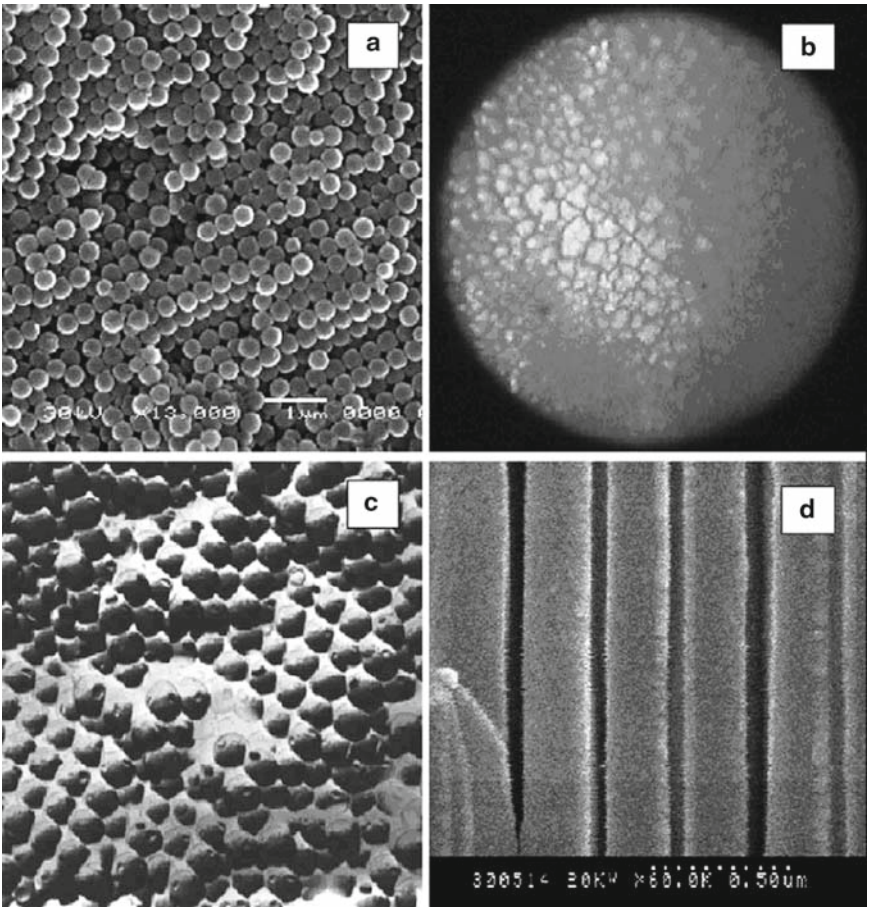

Fig. 6.12 Images of (**a**) opal matrix, (**c**) Er^{3+}-doped opal matrix, and (**d**) porous anodic alumina obtained by electron microscopy; (**b**) image of opal film obtained by optical microscope (Reprinted with permission from [220]. Copyright (2005) Elsevier)

each "written" mark contained up to 500 fluorescent beads. Later, they reported another study in which the full potential of the nanocomposite was realized by using every photo-sensitive core particle as a bit storage bin. Two-photon fluorescent dye excitation was employed to induce local photo- bleaching of the fluorescent micro-beads. The effective optical storage density was increased by a factor of two over conventional bulk materials. Figure 6.13 [221] shows the intensity distribution of a bit pattern photo bleached in homogenous material and nanostructured material composed of fluorescent particles.

In general, the major advantages of using nanocomposites in 3D optical data storage applications include [10, 41, 219, 221, 223]:

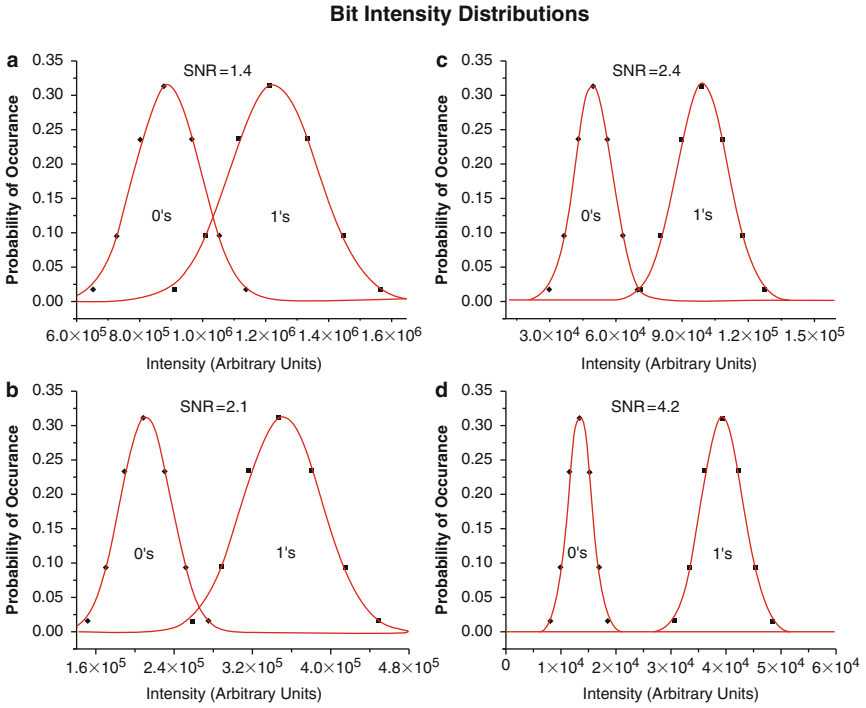

Fig. 6.13 Bit intensity distributions in the material with a homogenous structure (**a, b**) and the nanostructured material (**c, d**) (Reprinted with permission from [10]. Copyright (2001) AIP)

(1) Nanocomposites provide a greater flexibility in the design of new recording media compared to homogeneous materials. The rigid latex cores can be replaced with two-layer particles composing of a fluid core and a thin rigid shell, where the fluid core is synthesized from a low-*Tg* polymer. Since the high viscosity of polymers above the glass transition temperature imposes a significant barrier to photochemical processes involving molecular rearrangements or bimolecular processes (atomic displacements in general), the photochemical reactions in the fluid cores will occur at higher speeds [227]. Hence, the quantum yield increases significantly in fluid environments and accordingly, the write speed.
(2) Spatially periodic modulation of the photosensitive material.
(3) Significant reduction in the cross talk in writing and reading processes that results from the compartmentalization of information carrying domains with respect to optically inert regions, which create "dead space" barriers against cross talk.
(4) Additional filter mechanism and ability to better tune the photochemistry within composite materials makes nanocomposite polymeric systems highly attractive candidates as future high density optical storage media [221].

Another major application of photopolymers is with respect to the development of holographic data storage devices because of their high sensitivity and large refractive index change [228]. They have been extensively investigated as holographic recording media for many applications, including holographic scanners, LCD displays, helmet-mounted displays, optical interconnects, waveguide couplers, holographic diffusers, narrowband wavelength filters, laser eye protection devices, automotive lighting, and security holograms [226, 228–230].

Holograms are stored in photopolymer materials as spatial modulations of refractive index created in response to an interference pattern generated by incident laser beams. Because of photoreactions, the refractive index of irradiated areas of a material differs from that of dark areas. The bigger the difference in the refractive index between these two regions, the greater will be the data storage capacity of the material. The storage capacity of the material is also enhanced if the medium is thick, as this enables recording of many holograms in a given volume of material and results in improved diffraction efficiency of phase grating (modulated index) [226, 228–230].

Among the photopolymers, an organic–inorganic hybrid film is proposed to yield rigid media with low dimensional changes during holographic recording. Further, optical transparency and ease of film processing with sol–gel solutions for the organic–inorganic hybrids ensure the preparation of a thick film [228]. Many researchers showed that inclusion of nanoparticles contributed to rapid grating build-up and noticeable suppression of polymerization shrinkage, yielding high recording sensitivity and dimensional stability. The grating formation in nanoparticle-dispersed photopolymers is explained in terms of the mutual diffusion of monomer molecules and nanoparticles during holographic exposure because reactive monomer is consumed more in the bright region than in the dark one under holographic illumination and monomer molecules diffuse from the dark to the bright regions due to the difference of chemical potential between the bright and the dark regions. At the same time nanoparticles counter-diffuse from the bright to the dark regions. This is because the chemical potential of nanoparticles becomes higher in the bright region owing to their photo-insensitivity. As a result, compositional and density modulations of the formed polymer and nanoparticles having different refractive indices are spatially created, leading to the formation of a refractive index modulation (Δn) as large as 10^{-2} [226].

Transparent inorganic oxides such as TiO_2 and ZrO_2 possess refractive indices much higher than those of available monomer and polymeric binder materials (>2) in the visible region: e.g., bulk refractive indices of 2.55 and 2.1 at 589 nm for TiO_2 and ZrO_2, respectively. Therefore such high-refractive-index inorganic nanoparticles may be used to increase Δn further [226]. In these photopolymer nanocomposite films, holographic recording is achieved through photo-induced refractive index contrast arising from a compositional variation induced by polymerization and the subsequent diffusion of monomers into the polymerized areas (the high-intensity region of irradiation, the bright region) of the film under the constructive and destructive interference of multiwaves [228]. Achieving the desired storage capacity that would make holographic data storage commercially viable (~100 bits/μm^2)

will therefore require developing a large index contrast in thick photopolymer materials [230].

Suzuki et al. proposed holographic photopolymer incorporated with inorganic TiO_2, SiO_2 and organic (hyperbranched polymer) nanoparticles for permanent volume holographic storage with high diffraction efficiency [220, 231–233]. TiO_2 nanoparticles with an average diameter of 15 nm dispersed in methacrylate photopolymers gave Δn as large as 5.1×10^{-3} and the polymerization shrinkage suppression of approximately 69% was achieved at the nanoparticle concentration of 15 vol%. Sanchez et al. [234] also reported a similar 4 nm (average diameter) TiO_2 nanoparticles dispersed in the mixture of two kinds of acrylate monomers. They performed holographic recording at a wavelength of 351 nm and obtained Δn as large as 15.5×10^{-3} at 633 nm. However the systems reported by both Suzuki et al. and Sanchez et al. suffered scattering losses as high as 20 and 29%, respectively, for the 40 μm film thickness.

Further development of modern optical devices for information storage, transfer, and processing requires a transition from "classical" optical media to materials with quantum-dimensional parameters, in which an interaction of optical radiation with medium on interfaces of the medium play the fundamental role [219]. Such an approach results in considerably modified optical characteristics of materials, in particular, a substantial increase in the optical response of the medium. New possibilities are open for creating advanced devices for telecommunications and other modern industrial segments.

6.2.6 Light Emitting Diodes (LEDs)

LED technology is being used in commercial applications such as small screens for mobile phones and portable digital music players (MP3 players), car radios and digital cameras and also in high resolution micro displays for head-mounted displays. Organic light emitting diodes are found in models of the Sony Walkman and of some of the Sony Ericsson phones, notably the Z610i, as well as most Motorola color cell phones [47].

6.2.6.1 Si-Based Nanocomposite Materials in LEDs:

Efficient visible photoluminescence from etched and as-anodized porous silicon and observation of a blue shift in absorption edge triggered attention on the optoelectronic behavior of nano-sized silicon from the view-points of scientific and technological interests [235]. Fig. 6.14 [2] shows a nanostructured composite of silicon quantum dots in an amorphous matrix. Although Si is the base material of modern microelectronics, unfortunately, it does not efficiently emit light, due to its indirect band gap and the exciton binding energy of a few meV. Photoluminescence (PL) from Si is observed only at low temperature, which makes it impractical for

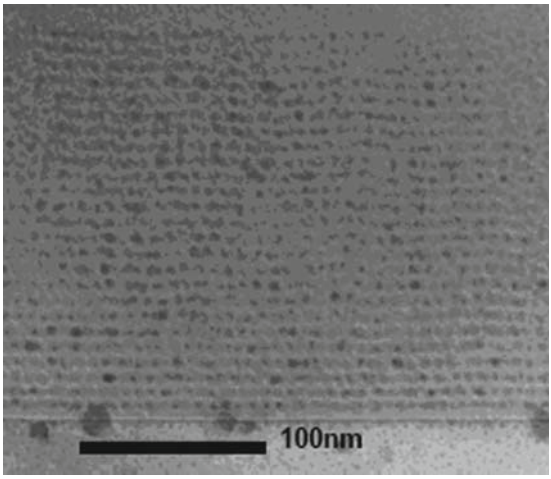

Fig. 6.14 TEM image of nanostructured silicon quantum dots in an amorphous matrix for photovoltaic applications. (Reprinted with permission from [20]. Copyright Proceedings of ACUN-5 International Composites Conference: Developments in Composites: Advanced, Infrastructural, Natural and Nanocomposites, Sydney)

use in optoelectronic circuits and devices. To overcome this problem and to achieve high emission yield from Si, several different systems have been proposed [11, 236–240] and one among such systems is based on nanostructured Si (nanocrystalline and porous Si), where quantum confined effects and exciton localization play a major role in the light emission process [238, 239].

Silicon nanocrystals as a light source had an additional advantage over bulk silicon in that the electrical carriers were confined to a region in which no defects were present due to the fact that the host material (normally SiO_2) ensures an efficient passivation of defects and recombination centers. This opened gates for different systems based on Si and SiO_2 to be investigated, like SiO_2 layers doped with Si nanocrystals [238], Si/SiO_2 superlattices [11], oxidized porous Si or single nanometer-thick quantum wells of crystalline silicon. Above all, the insulating effect of SiO_2 makes it even difficult to inject electrical charges into Si nanocrystals, and thus efficient light-emitting diodes are troublesome to make. Moreover, large currents passing through an oxide film will eventually make it fail, resulting in a short circuit. Amato et al. [4] proposed a completely different approach to produce Si/SiO_2 nanocomposites by investigating the possibility of infiltrating Si into porous silicon oxide (PSO) by CVD. PSO in which the pores are interconnected acted as a template for the growth of the Si network so that the complete pore filling gives rise to a percolated Si network inside SiO_2. The authors reported that the system was absent of consequent effects to porosity such as instability, reactivity, and fragility. Additionally, several alternative ways have been pursued to deal with its inability of Si to luminescence efficiently. Some examples are crystalline silicon doped with rare earth ions, crystallized silicon quantum dots

[240], and porous silicon [239]. Luminescent PS layer (formed by anodic conversion of single-crystal silicon c-Si) consists of highly packed, isolated and/or interconnected silicon nanocrystallites with a mean diameter of 2–3 nm, which is below the critical level for the occurrence of quantum confinement. Koshida and Gelloz [235] reviewed wet and dry porous silicon, their characterization, and properties at greater depth.

In addition, silicon-based materials were also used as hosts for erbium doping. They showed a 1.54 μm emission (falls in the window of maximum transmission for silica-based optical fibers) stimulating both academia and industries on erbium-doped materials. 4f-shell luminescence from erbium-doped crystalline silicon was reported for the first time in 1983 [2], and after that, erbium has been incorporated in numerous other materials. Porous silicon was also used as a host for the incorporation of erbium ions. The ability to manufacture high reflectivity multilayer structures [238], efficient visible photoluminescence [239], and compatibility with standard silicon processes in making integrated optoelectronic devices [11] has attracted porous silicon. The large surface area of nanostructured matrix of porous silicon allows easy infiltration of the ions into the matrix. The structure of porous silicon readily oxidizes, producing large concentrations of oxygen necessary for efficient erbium emission. Different doping techniques have been proposed for porous silicon, such as ion implantation [241], diffusion [242], and electrochemical migration [243]. Among these, cathodic electrochemical migration was preferred because it offers the advantages of deeper erbium penetration (10–20 μm), lower cost, and simplicity of processing. However, erbium-doped crystalline silicon structures were usually prepared by expensive and time consuming processes like ion implantation, epitaxial growth, and chemical vapor deposition, which also require specialized equipment, and limited to very shallow doping profiles [4].

Lopez et al. [244] infiltrated erbium in the pores by cathodic electrochemical migration of the ions followed by high temperature annealing (600–1,100°C) to produce a composite material made of silicon nano-crystals and silicon dioxide. The devices exhibited exponential electroluminescence dependence in both bias conditions (Fig. 6.15 [244]) as a function of the driving current and driving voltage. It was reported that in reverse bias, the external quantum efficiency reached 0.01%; the electroluminescence intensity decreased by a factor of 24 in reverse bias and 2.6 in forward bias when the temperature increased from 240 to 300 K; and the photoluminescence from the erbium-doped micro cavity resonators was enhanced by more than one order of magnitude and tuned to emit in areas where the natural erbium emission was very weak.

6.2.6.2 Polymer-Based Materials in LEDs

Polymers are very promising candidates for cost-effective micro- and nano-photonic devices in optical communication networks, chip-to-chip interconnections and sensors. They have many desirable properties, such as easy fabrication, low production cost, device integration, and compatibility with Si and GaAs fabrication

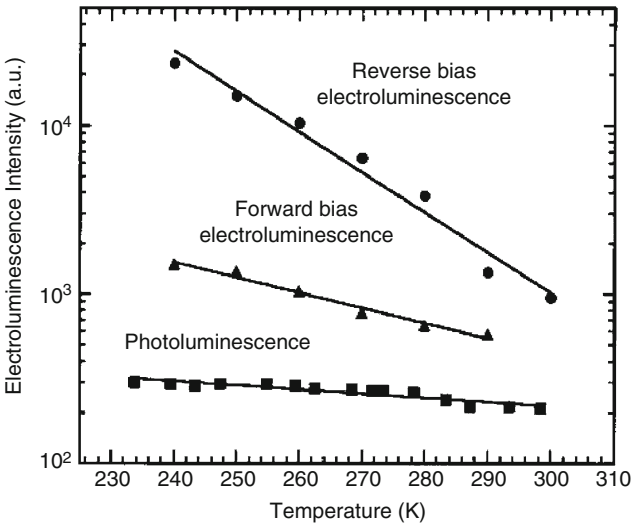

Fig. 6.15 Temperature dependence of photoluminescence and electroluminescence under forward and reverse bias. Data for electroluminescence was taken at a constant current density of 34 mA/cm^2 (Reprinted with permission from [165]. Copyright (2001) Elsevier)

technologies [245]. They can also be deposited directly on any kind of substrates and tune their optical properties by different combinations of monomers and dopants. Different classes of polymers have been developed for micro-photonics: photosensitive polymers (e.g., polyimides and photoresists), olefins, fluorinated polymers, acrylates, elastomers [245].

π-conjugated polymers are extensively studied for their potential use in light emitting diodes, photovoltaic cells (solar cells), and organic thin-film transistors. Poly(*p*-phenylene vinylene) (PPV) and its derivatives were promising in this regard because of their particular structure and highly interesting electroluminescent, electrical, nonlinear optical and lasing properties [246]. Besides PPV and its derivatives, polyfluorene (PF) and its derivatives are promising conjugated polymers for PLEDs because of their thermal and chemical stability, good solubility, and high fluorescence quantum yields. Despite this, the use of PF and its derivatives for PLED applications has several disadvantages arising from the aggregation and excimer formation and/or thermal oxidation (keto defect), as well as intermolecular cross-linking between PF chains. These include relatively low electroluminescence quantum efficiencies and unstable color purities. Although many approaches were used to overcome these problems, like introducing solubilizing substitutes to control the aggregation, there are still problems like complicated synthesis process and difficult to access fully aromatic materials. Thus, further improvements are still needed to achieve the commercialization of full-color displays [247] demonstrating the need for more stable and efficient conjugated polymers.

An alternate approach to polyaromatics with multiple advantages in terms of ease of synthesis, robustness, versatility in functionality, and high solubility was

reported by Brick et al. [26]. Cubic octasilsesquioxanes novel compounds are used as model catalytic surfaces, molecular catalysts, porous media, NMR standards, fluoride encapsulants, and building blocks for nanocomposite materials. They reported that polybromophenylsilsesquioxane $Br_{5.3}$OPS reacts readily with borates of phenyl, biphenyl, naphthyl, 9,9-dimethylfluorene, and thiophene using standard Suzuki conditions to produce the corresponding polyaromatic and heteroaromatics with complete substitution of all bromines. The resulting materials were completely soluble in a variety of common organic solvents and were also stable at temperatures exceeding 400°C in air. Photoluminescence measurements showed standard aromatic behavior with typical quantum efficiencies [26].

Polyhedral oligomeric silsesquioxanes (POSSs), have unique cube-shaped molecular structure and nanoscale dimensions, and POSS-functionalized organic–inorganic hybrid materials were used as modifiers for nanoparticle applications [247]. POSS-substituted organic–inorganic hybrid PFs were also developed by several groups. Lee et al. [247] reported POSS-pendant PF copolymers and showed that they have higher luminescence, efficiency, and color stability than POSS-free pristine PF. Later, they hypothesized that small amounts of nanoscale POSS attached to the C-9 position of fluorine in PF derivatives would reduce the intermolecular π–π interactions between polymer chains and thus suppress aggregation and thermal oxidative degradation [247]. Also, photoluminescence and electroluminescence studies of POSS-functionalized PF derivatives showed that the inclusion of POSS strongly suppresses the intermolecular aggregation and thermal oxidation and thus, enhanced the light-emitting performance.

Recently, super radiance in PPV and PPV analogues was achieved suggesting the prospect of polymer semiconductor lasers [246]. PPV exhibits a strong two-photon pumped up-conversion emission when excited by near-IR laser pulses of 800 nm, which also opens up another prospect, upconversion lasing [246]. PPV is traditionally made by a base catalyzed reaction of a water-soluble salt monomer precursor. However, many questions and difficulties still remain in spite of the rapidity with which PPV has been developed for electroluminescence applications. It is extremely difficult to achieve a narrow distribution of molecular weight of PPV due to the difficulty in controlling the base-catalyzed reaction and therefore leads to large polymer chains. Moreover, since the final polymer is insoluble, it is difficult to process it in various forms such as a bulk sample or in the form of a blend with other polymers. Lal et al. [246] demonstrated a controlled, nanoscale polymerization of the PPV monomer conducted within the size-controlled cavity of reverse micelles, which yields processable PPV. These PPV analogues (oligomers) were also readily processed through dispersion to prepare polymer blends. Figure 6.16 [246] shows the Fluorescence emission from poly(*p*-phenylenevinylene) of different conjugation lengths synthesized within reverse micelles. Ho et al. [248] demonstrated that PPV-SiO_2 nanocomposites exhibited a composition dependence of refractive index that can be utilized to fabricate all polymer photonic structures in the visible-NIR region. They fabricated conjugated polymer distributed Bragg reflectors and micro-cavity light-emitting diodes [176, 248]. In this PPV-SiO_2 system, a very large refractive index contrast was also achieved (>40%). This system also has other advantages such as:

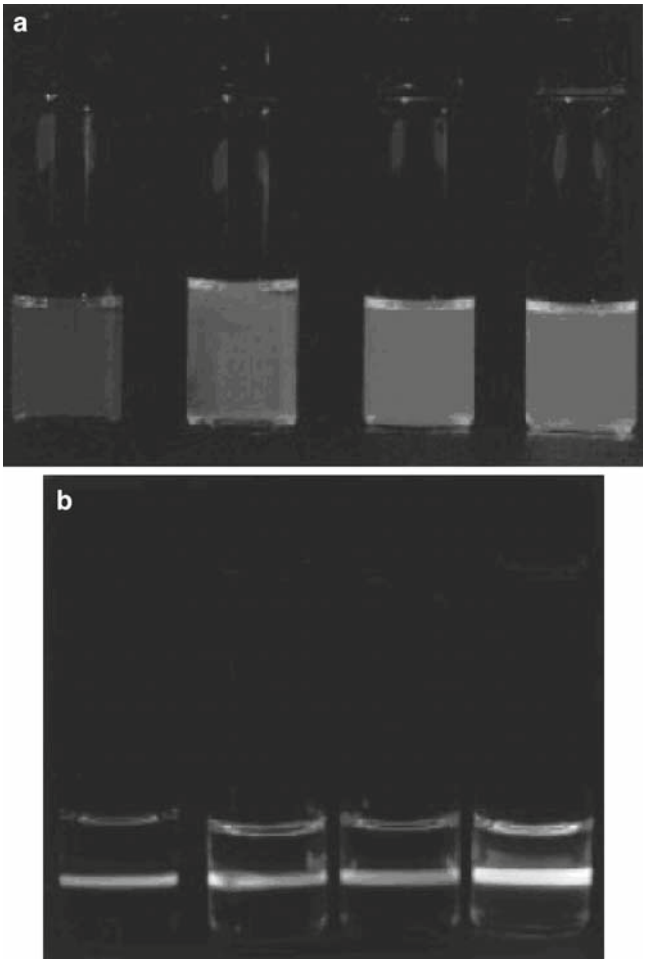

Fig. 6.16 Fluorescence emission from poly(*p*-phenylenevinylene) of different conjugation lengths synthesized within reverse micelles (from left to right: W_0 = 5, 10, 15, 20). (**a**) UV excitation; (**b**) two-photon excitation at 800 nm (Reprinted with permission from [108]. Copyright (1998) ACS)

(a) silica is transparent over the key electronic and vibrational bands of PPV, also inert to the acidic thermal elimination reaction that generates PPV,
(b) silica is a wide band gap insulator (hydrolytic silica is expected to have few chemical defects; e.g., dangling bonds, so neither bulk/surface charge trapping nor excitation energy transfer occurs)
(c) spectroscopic properties of PPV and its oligomers are well characterized and
(d) simple repeat structural unit of PPV leads to sharp spectroscopic features that are more sensitive to disorder than those of many other conjugated polymers.

In the light-emitting diodes made of *p*-type polymers such as PPV derivatives, the majority of the carriers of the emissive polymers are holes. It is thus, necessary to

improve the electron injection ability at the interface of the polymer cathode and to block the holes effectively before they reach the cathode, to improve the EL quantum efficiency. For this purpose cathodes with low work function such as Ca and Mg have been employed [247]. Since metals are susceptible to degradation upon exposure to air an inert atmospheric condition is required to deal with them. To overcome this problem, an electron injecting or transporting layer or an insulating layer such as Al_2O_3 and LiF were employed for the stable and efficient EL device with an Al cathode. Later, the EL device with Al cathode was greatly improved by the post-deposition annealing above the glass transition temperature of an emitting polymer without any additional layer. A quantum well structure for the charge confinement was also employed to improve the electron-hole recombination rate of the organic EL device by An et al. [249]. In spite of all these efforts, fabrication of multilayer devices by successive spin casting of polymer solutions is not easy. Hence, to commercialize the polymeric EL devices the improvement of device stability was urgently required.

Both chemical and physical methods were used to enhance the performance of PPV-based devices. Using chemical methods, structure of the polymer was changed by adding functional groups to the backbone, thereby improving the solubility or modifying the band gap of the material [250]. Although, the chemical techniques gave good results, they strongly depend on the synthesis of the polymer. Regarding physical methods, the properties of a polymer can be improved by adding "selective" inorganic nanoparticles to the host material and this process is also believed to increase the electrical conduction of the polymer, and in addition, improve its stability. Many researchers have reported nanocomposites of silica/titania nanoparticles with PPV or its derivatives [251, 252]. Silica nanoparticles had a good effect on the conductivity of the polymer host while the titania nanoparticles influenced photovoltaic properties. In both cases, modification of the polymer luminescence was observed. However, contradictory results were reported in very similar materials; for example poly(2-methoxy-5(2′ ethyl) hexoxy-phenylene vinylene) blended with SiO_2 was found to have an improved conductivity as compared to the bare polymer; while PPV with similar nanoparticles showed a lower conductivity than the polymer alone. Lee et al. [251] reported that conjugated polymer layered silicate nanocomposites with high environmental stability against oxygen and moisture showed greatly improved photoluminescence intensity and its EL device also possesses hugely improved external quantum efficiency. Nguyen et al. [252] performed isolation of a conjugated polymer chain within mesoporous silica to control chain conformation and energy migration. It was also reported that the conjugation length of the polymer could be altered by the incorporation of the nanoparticles, modifying its optical and electrical properties [250]. The main consideration here should be that the polymers used in these works were not synthesized by the same technique and the analysis of the results should also mind the quality of the polymer materials.

Yang et al. [250] studied diodes made using PPV/SiO_2 and PPV/TiO_2 nanocomposites by depositing the composite thin film onto indium tin oxide (ITO) substrates followed by thermal evaporation of a MgAg cathode of thickness 500 nm. Figure 6.17 [250] represents the current density vs. applied field for devices with different concentrations of PPV/SiO_2 and PPV/TiO_2 composites.

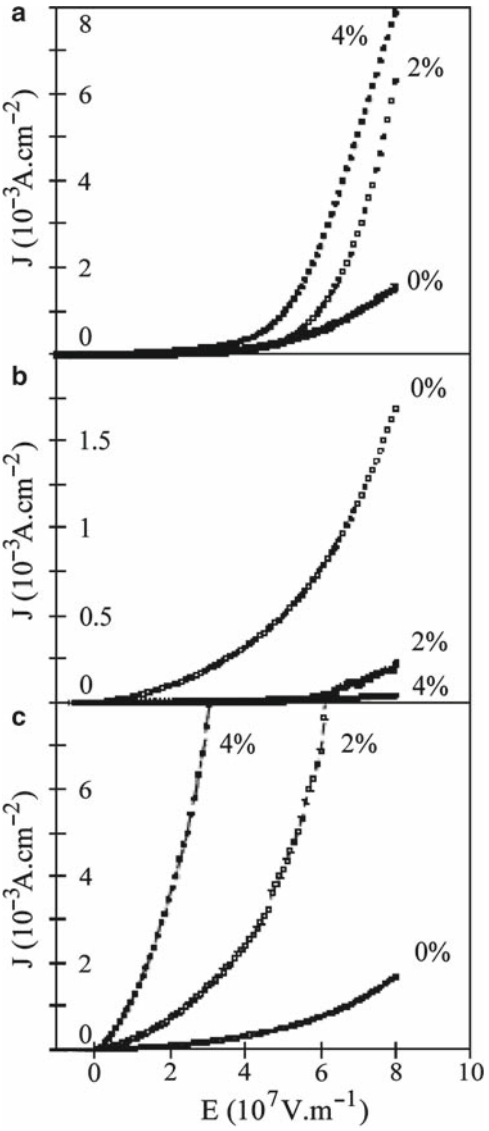

Fig. 6.17 Current density vs. applied field in diodes with different nanoparticle concentrations: (**a**) ITO–PPV/SiO_2 (100 nm)–MgAg; (**b**) ITO–PPV/SiO_2 (20 nm)–MgAg; (**c**) ITO–PPV/TiO_2 (20 nm)–MgAg (Reprinted with permission from [137]. Copyright (2005) Elsevier)

The authors reported different behavior patterns in devices of PPV/SiO_2, depending on the particle sizes; for smaller particles, the conductivity of the composite decreased with the increasing concentration, while for larger particles, it increased with the concentration. Qian et al. [253] showed almost forty times increase in photoluminescence from nanotubed titania, compared to that of nanoparticles. This increase was attributed to the translational symmetry in TiO_6 octahedron that remains along the tube axis; and no longer exists around its circumference.

Since nanoparticles and nanotubes have different characteristics of surface area, morphology, etc, the changes in the electronic band structure resulted in increasing luminescence of titania nanotubes. They also reported blue electroluminescence from titania nanotubes [253] doped into a poly (2-methoxy-5-(2-ethyl hexyloxy)-*p*-phenylene vinylene) (MEH-PPV) matrix which directly comes from band to band transitions of titania nanotubes. The onset voltages of the polymer light-emitting diodes were lowered after doping with titania nanotubes and the doped devices gave higher current compared with the undoped ones. Figure 6.18 [253] shows the normalized EL spectra of the PLEDs.

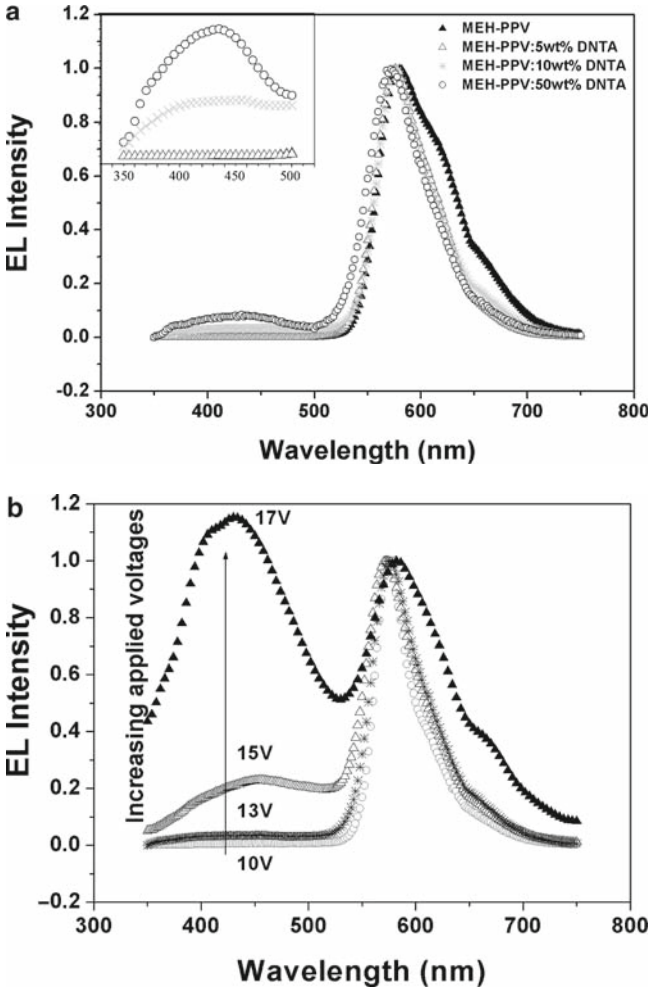

Fig. 6.18 (**a**) Normalized EL spectra of PLEDs with different concentrations of titania nanotubes (applied voltages at 13 V). (**b**) Normalized EL spectra of PLEDs doped with titania nanotubes at weight ratio 10 wt% under different applied voltages (Reprinted with permission from [31]. Copyright (2006) Institute of Physics)

Effective charge confinement of the nanocomposite devices plays a critical role in improving the luminescent efficiency. Lee et al. [254] determined the charge (electronic and ionic) carrier mobility of the LED made of nanostructured polymer/clay composites by measuring pulsed- and steady-state transient EL. The authors reported that the clay within the nanocomposite acted as a barrier against both electronic and ionic charges. Figure 6.19 [254] represents the transient current and EL as a function of time of different devices for a steady state electric field.

Furthermore, conducting polymer nanostructures not only have advantages/applications in light emitting diodes, but also in various other electronic devices such as flexible electronic circuits, field effect transistors and so on due to their ease of controlling the conductivity (from insulator to conductor) by changing the doping level. However, Lewis acid a commonly used dopant is reactive enough to damage the electronic devices limiting long lifetime and device stability. On the other hand,

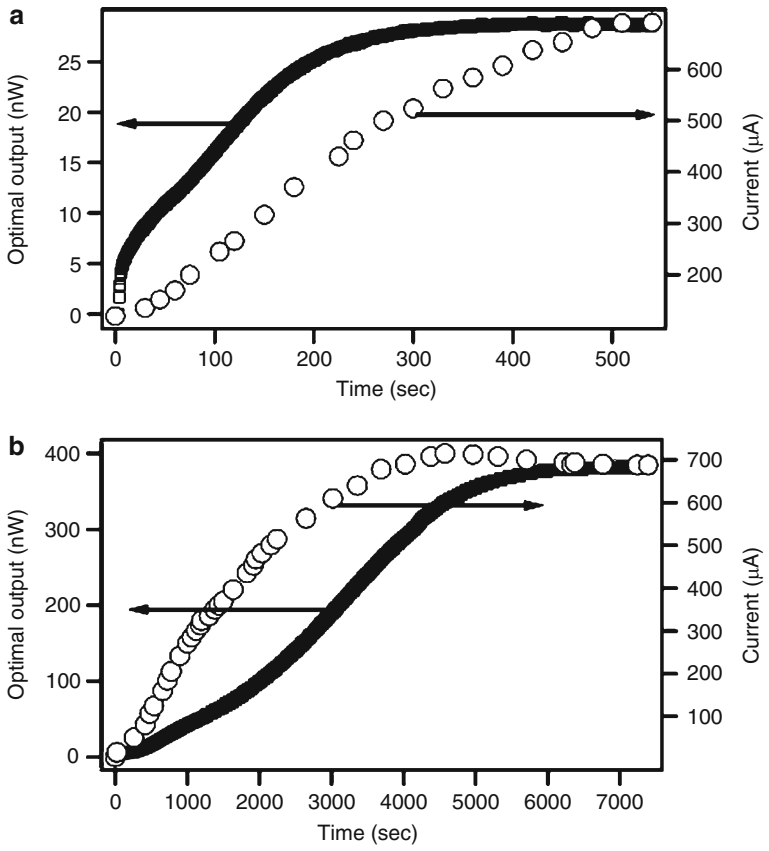

Fig. 6.19 Transient current and EL as a function of time while applying a steady state electric field (9.5×10^7 V/m). (**a**) ITO/MEH-PPV/Al; (**b**) ITO/(MEH-PPV/Clay)/Al (Reprinted with permission from [201]. Copyright (2001) Elsevier)

small organic compounds have been applied to the semiconductors capable of being fabricated into thin-film transistor (TFT). Examples include oligothiophenes, substituted naphthalenes, phthalocyanines, and pentacene. The conduction mechanism for these classes of organic semiconductors involves charge transport across π electrons in these molecules. Most of them are known to carry electrons by positive charge (hole). Triphenylamine derivatives such as *N,N′*-bis-(4-methylphenyl)-*N, N′*-diphenylbenzidine (TPD), transport hole were used as organic conductors or in organic electroluminescence devices. A new method to fabricate semi-conductor by solution process based on the composite of organic hole transporting compound, TPD, and titanium dioxide (TiO_2) nanoparticles by sol–gel process was reported by Yokozumi et al. [255]. The conductivity of the composite increased up to six orders of magnitude higher than that of TPD itself when TPD was doped with TiO_2 nanoparticles.

In sum, multifunctional polymers (exhibiting simultaneously more than one property) are a new generation of materials that hold considerable promise for numerous applications in the field of electronics and photonics [246]. Manipulation of molecular architecture and the morphology at nano level provides a powerful approach to control the electronic and optical properties of a material as well as its processability. So far, most of the research was carried out on inorganic semi-conductors in the design and preparation of quantum confined structures such as quantum dots, quantum wires, and quantum wells [246]. Electron-hole pairs can be quantum confined to control the band gap of materials by the correct choice of physical sizes. In case of inorganic materials (semi-conductors and metal clusters) the electronic and photonic properties, which are strongly dependent on their band gaps, are well documented. However, nano-scale processing of polymers in a restricted geometry to produce quantum confined structures and composites is less explored. By tuning the morphologies, band gaps, and charge-transport properties of these polymers, device stabilities have been increased, and emitters at a wide variety of wavelengths have been fabricated [246, 251, 254, 256, 257].

6.2.7 Miscellaneous Applications

6.2.7.1 Ultra Large Scale Integration (ULSI) Devices

Multilayer polymer ceramic structures are important for many applications such as the need for thin film polymers for electronic packaging, coatings, passivation layers, lubrication, biocompatible materials, and intermetallic dielectrics for ULSI devices. [258]. A major need exists to replace silicon dioxide with a low dielectric constant material such as a polymer to reduce RC-delay and cross-talk in integrated circuits. However, to realize this goal both synthesis techniques and a fundamental understanding of polymer thin films are needed. Different integration schemes were proposed which used SiO_2 and functionalized poly(*p*-xylylene) derivatives to take advantage of silica's good adhesion properties and thermal stability while also

taking advantage of the polymer's low dielectric constant, which would ultimately reduce the RC-delay in ULSI devices [258, 259]. The presence of SiO_2 specific interactions and physical confinement causes thin film polymers to have more complex morphology compared to the complex anisotropic morphology of the polymers. Crystallization behavior of the polymer is a noticeable effect of the specific interactions. In this regard ultrathin films of polystyrene (formed by spin casting/coating technique) on H-terminated Si and on native oxide silicon have been studied and it was reported that they exhibited opposite behavior in terms of their glass transition temperature as a function of film thickness [258, 259]. These polymeric films are not advantageous in fabricating ULSI devices due to their low processing throughput, poor conformality, purity incorporation and the presence of casting solvent, which is an environmental concern. Senkevich et al. [258] have deposited both SiO_2 and PPXC (poly (chloro-*p*-xylylene)) polymer layer at near room temperature by thermal CVD. CVD is very promising, but it is not very cost effective. They reported that the introduction of a polymer with SiO_2 raised the refractive index from 1.44 to 1.59 (at 630 nm) and lowered the dielectric constant from 4.0 to 3.30 (at 10 kHz) with a PPXC thickness fraction of ~0.80.

Ezhilvalavan and Tseng [260] reviewed the use of tantalum pentoxide (Ta_2O_5) thin films for ULSI circuits applications. They investigated the deposition of Ta_2O_5 films by reactive sputtering, photo- CVD (chemical vapor deposition) and LPCVD (low pressure CVD) and reported that LPCVD is more appropriate for high density device applications owing to its good step coverage. Also maximum dielectric constant and low leakage current density obtained with LPCVD-Ta_2O_5 films were better than those of other processing methods.

6.2.7.2 Liquid Crystal Displays (LCDs)

Nanocomposites consisting of spatially confined liquid crystals are of great interest due to the prospects of their application in optoelectronic devices, photonic crystals, depolarizers, scattering displays, information storage and recording devices, and windows with adjustable transparency. In these systems, applied external electric field causes switching between the scattering and transparent states, and, under some conditions, these states can be retained after the field switching off. In case of spherical aerosol particles, it was found that the memory effect is achieved due to formation of ordered branched network of the aerosol particles in the liquid crystal matrix. But in the case of anisometric particles of a clay mineral an important contribution for the memory effect can be from the influence of the clay surface on the alignment of adjacent liquid crystal (LC) layers, which can be controlled by the application of hydrophobic organic modifier on the clay mineral.

The effect of modification of the montmorillonite (MMT) clay mineral with different organic surfactant ions on the electro-optical properties of the MMT + 5CB (4-pentyl-4′-cyanobiphenyl nematic liquid crystal) heterogeneous LC–clay nano systems have been studied by Chashechnikova et al. [261]. Using IR and Raman

spectroscopy techniques, it was shown that in the LC-clay nanocomposites consisting of organically modified MMT and 5CB, mutual influence of 5CB molecules and the clay particles occurred that resulted in the ordering of the near-surface layers of both inorganic and organic components of the composites. Because of this Van der Waals interaction, the system became transparent under the action of electrical field, and preserved the transparent state when the voltage was switched-off, i.e., the contrast and electro-optical memory effect were observed. They also reported that the use of polar additive (acetone) for preparation of the nanocomposite increases the uniformity of the composites and considerably improves their electro-optical properties.

6.2.7.3 Flat Panel Displays

The velocity of electrons approaching the speed of light (3×10^8 ms^{-1}) in vacuum is limited to only a saturation velocity of 10^5 ms^{-1} in solids by lattice scattering; thus, making vacuum electronic devices attractive for high speed and high frequency applications [262]. Conventional vacuum electronic devices use electrons liberated by thermionic emission from hot filaments that are large and need much energy in heating up the filament. So, replacing the thermionic cathode by a cold cathode (uses field emission, FE, electrons where the electrons are liberated by tunneling from the cathode material at room temperature under intense electric field) can reduce the size of the device and also improve the power efficiency. Cold electron FE materials, with low threshold fields, are seen as potential candidates for flat panel displays (FPD). Some of the novel cold field emission materials include metallic-dielectric nanocomposites such as resin-carbon coatings [263, 264] graphitic clusters embedded in amorphous carbon (a-C) films, metal doped a-C films and metal implanted SiC layers [264]. Due to a local electric field enhancement by virtue of the electrical inhomogeneity between nano-sized conductive clusters and insulating dielectric matrix, these materials have excellent field emission properties and very low threshold fields for electron emission, smaller than 20 V/μm compared to several thousand volts per micron values of flat metallic cathodes.

Tsang et al. [264] have studied the electron field emission properties of the Ag–SiO_2 nanocomposite layers. Threshold fields as low as 13 V/μm was reported. Figure 6.20 [264] shows the electron field emission characteristics of the nanocomposite layers at different Ag doses. SiO_2 as a host matrix has the advantages of chemical stability, efficient fabrication process by thermal oxidation, and fast well characterized etching process of SiO_2 which is convenient to create differently patterned FE devices. Ag has excellent electrical and thermal conductivities (beneficial in FE device applications), does not react chemically with the SiO_2 matrix, and the formation of nano-sized pure Ag clusters in silica is possible with small Ag doses (1×10^{15} cm^{-2}) [264]. Hence, the combination of Ag–SiO_2 has the added benefit that the whole fabrication process is compatible with existing IC technology and thus the nanocomposite layers as the cathode material for vacuum microelectronic devices take advantage of the possibility for integrating the devices with other circuit elements on a single chip.

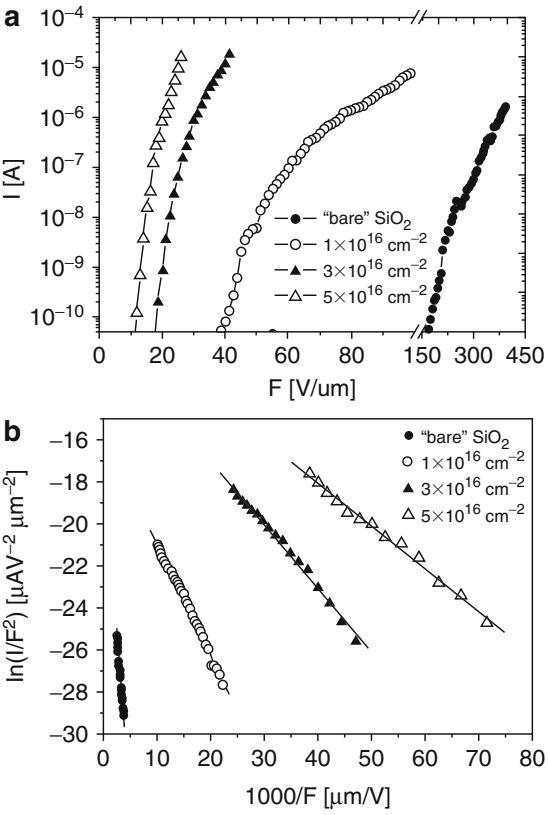

Fig. 6.20 Electron field emission characteristics of samples implanted with various Ag doses. (**a**) *I–F* characteristics and (**b**) the corresponding Fowler-Nordheim plots (Reprinted with permission from [175]. Copyright (2005) Elsevier)

6.3 Summary

In this chapter, we discussed the material aspects of some of the nanocomposites used in different electronic applications as: embedded capacitors, integrated circuits, lithium ion batteries, transistors, light emitting diodes, ULSI devices, LCDs, and flat panel displays. The potential of these hybrid materials has been realized in various modern day applications like: iMac G5 by Apple® Inc., OLEDs (Nanohorizons®, Motorola®, NUVUE AM55OL by Eastman Kodak®, Dupont®, Samsung®, Sony® corporation, Universal display corporation®, RiT display corporation®), Pioneer® organic electro luminescent display (OEL), Sanyo® OEL display, surface conduction electron emitter display by Canon®, television display coating by ecology coatings®, and in processors (Athlon® AMD™ 64 FX, AMD™ Athlon® 64 X2 dual-core, IBM power PC 970 FX/970 MP, Intel® Celeron® 4, Intel® Core™ duo, Intel® Pentium® 4, Intel® Pentium® D) [22, 265].

Nonetheless, it is evident from this review and the unwanted break downs in consumer electronics that more studies should be focused towards the fundamental understanding of these materials. Recall that with increasing ceramic loading, the dielectric constant of polymer/ceramic nanocomposite materials was increased for embedded capacitor applications, but the role of processing methods and conditions, filler size, shape, orientation, dispersion, percolation, and crystal structure are still not very clear. Likewise, nanoparticle dispersion is another critical issue that controls the use of these materials for commercial applications. Although, the research work discussed in this review is mainly oriented in terms of electronic behavior of the nanocomposites, it is very important to consider other properties of these materials (mechanical, thermal, rheological, or any combination there-of) in order to preserve the structural integrity of the material as a whole.

Acknowledgments S.K. Samudrala acknowledges University of New South Wales for the Visiting Fellow Position in the School of Materials Science and Engineering. Permissions from various publishers and authors to reproduce tables and figures in the manuscript are much appreciated.

References

1. Baibarac M, Gomez-Romero P (2006) Nanocomposites based on conducting polymers and carbon nanotubes: from fancy materials to functional applications. Journal of Nanoscience and Nanotechnology 6:289–302
2. Green MA (2006) Synthesizing semiconducting material using silicon – a nanostructured composite of silicon quantum dots in an amorphous matrix. In: Bandyopadhyay S, Berndt CC, Rizkalla S, Gowripalan N, Matisons J, Zeng Q (eds) ACUN-5 International Composites Conference: Developments in Composites: Advanced, Infrastructural, Natural and Nanocomposites Sydney, pp 513–518
3. Sanchez C, Julian B, Belleville P, Popall M (2005) Applications of hybrid organic-inorganic nanocomposites. Journal of Materials Chemistry 15:3559–3592
4. Amato G, Borini S, Rossi AM, Boarino L, Rocchia M (2005) Si/SiO2 nanocomposite by CVD infiltration of porous SiO_2. Physica Status Solidi A-Applications and Materials Science 202:1529–1532
5. Baibarac M, Baltog I, Lefrant S, Mevellec JY, Chauvet O (2003) Polyaniline and carbon nanotubes based composites containing whole units and fragments of nanotubes. Chemistry of Materials 15:4149–4156
6. Besenhard JO, Hess M, Komenda P (1990) Dimensionally stable Li-alloy electrodes for secondary batteries. Solid State Ionics 40–41:525–529
7. Bhattacharya A, Ganguly KM, De A, Sarkar S (1996) A new conducting nanocomposite – PPy-zirconium(IV) oxide. Materials Research Bulletin 31:527–530
8. Bhattacharya SK, Tummala RR (2001) Integral passives for next generation of electronic packaging: application of epoxy/ceramic nanocomposites as integral capacitors. Microelectronics Journal 32:11–19
9. Caseri WR (2006) Nanocomposites of polymers and inorganic particles: preparation, structure and properties. Materials Science and Technology 22:807–817
10. Siwick BJ, Kalinina O, Kumacheva E, Dwayne Miller RJ, Noolandi J (2001) Polymeric nanostructured material for high-density three-dimensional optical memory storage. Journal of Applied Physics 90:5328–5334
11. Lockwood DJ, Lu ZH, Baribeau JM (1996) Quantum confined luminescence in Si/SiO_2 superlattices. Physical Review Letters 76:539–541

12. (a) Kim DS, Lee T, Geckeler KE (2006) Hole-doped single-walled carbon nanotubes: ornamenting with gold nanoparticles in water. Angewandte Chemie (International ed. in English) 45: 104–107
12. (b) Mahima S, Chaki NK, Sharma J, Kakade BA, Pasricha R, Rao AM, Vijayamohanan K (2006) Electrochemical organization of monolayer protected gold nanoclusters on single-walled carbon nanotubes: Significantly enhanced double layer capacitance. Journal of Nanoscience and Nanotechnology 6:1387–1391
13. Merhari L, Belorgeot C, Moliton JP (1990) Etch rate modeling for ion-irradiated nitrocellulose. Applied Physics Letters 57:2785–2787
14. Merhari L, Moliton JP, Belorgeot C (1990) Fourier-transform infrared study of ion irradiated nitrocellulose. Journal of Applied Physics 68:4837–4845
15. Merhari L, Lehue C, Belorgeot C, Bahna Z (1991) Ion-implantation profile modeling of nitrocellulose coated substrates. Applied Physics Letters 59:2856–2858
16. Merhari L, Belorgeot C, Moliton JP (1991) Ion irradiation induced effects in polyamidoimide. Journal of Vacuum Science & Technology B 9:2511–2522
17. Merhari L, Belorgeot C, Quintard P (1994) Helium ion-irradiated polyamidoimide films – a ft-ir and raman follow-up. Journal of Materials Science Letters 13:286–288
18. Merhari L, Gonsalves KE, Hu Y, He W, Huang WS, Angelopoulos M, Bruenger WH, Dzionk C, Torkler M (2002) Nanocomposite resist systems for next generation lithography. Microelectronic Engineering 63:391–403
19. Ogitani S, Bidstrup-Allen SA, Kohl PA (2000) Factors influencing the permittivity of polymer/ceramic composites for embedded capacitors. IEEE Transactions on Advanced Packaging 23:313–322
20. Ago H, Petritsch K, Shaffer MSP, Windle AH, Friend RH (1999) Composites of carbon nanotubes and conjugated polymers for photovoltaic devices. Advanced Materials 11:1281–1285
21. Bakueva L, Musikhin S, Sargent EH, Schulz S (2003) Fabrication and investigation of nanocomposites of conducting polymers and GaSb nanocrystals. Surface Science 532:828–831
22. http://www.intel.com/technology/silicon/65nm_technology.htm.
23. Amos SW, James MR (1999) Principles of Transistor Circuits. Butterworth-Heinemann, Oxford
24. Horowitz, Paul, Hill (1989) The Art of Electronics. Cambridge University Press, Winfield
25. Warnes L (1998) Analogue and Digital Electronics. Macmillan, New York
26. Brick CM, Ouchi Y, Chujo Y, Laine RM (2005) Robust polyaromatic octasilsesquioxanes from polybromophenylsilsesquioxanes, BrxOPS, via Suzuki coupling. Macromolecules 38:4661–4665
27. Kumar S, Pimparkar N, Murthy JY, Alam MA (2006) Theory of transfer characteristics of nanotube network transistors. Applied Physics Letters 88:123505 (1–3)
28. Kumar TP, Ramesh R, Lin YY, Fey GTK (2004) Tin-filled carbon nanotubes as insertion anode materials for lithium-ion batteries. Electrochemistry Communications 6:520–525
29. Philip B, Xie JI, Abraham JK, Varadan VK (2004) A new synthetic route to enhance polyaniline assembly on carbon nanotubes in tubular composites. Smart Materials & Structures 13: N105–N108
30. Torsi L, Cioffi N, Di Franco C, Sabbatini L, Zambonin PG, Bleve-Zacheo T (2001) Organic thin film transistors: from active materials to novel applications. Solid-State Electronics 45:1479–1485
31. Yao KJ, Song M, Hourston DJ, Luo DZ (2002) Polymer/layered clay nanocomposites: 2 polyurethane nanocomposites. Polymer 43:1017–1020
32. Yao ZL, Braidy N, Botton GA, Adronov A (2003) Polymerization from the surface of single-walled carbon nanotubes – preparation and characterization of nanocomposites. Journal of the American Chemical Society 125:16015–16024
33. Ree M, Goh WH, Kim Y (1995) Thin-films of organic polymer composites with inorganic aerogels as dielectric materials – polymer-chain orientation and properties. Polymer Bulletin 35:215–222
34. Ree M, Shin TJ, Lee SW (2001) Fully rod-like aromatic polyimides: Structure, properties, and chemical modifications. Korea Polymer Journal 9:1–19

35. Ree MH, Yoon JW, Heo KY (2006) Imprinting well-controlled closed-nanopores in spin-on polymeric dielectric thin films. Journal of Materials Chemistry 16:685–697
36. Kang S, Leblebici Y (2002) CMOS Digital Integrated Circuits Analysis & Design. McGraw-Hill, New Tork
37. Mead C, Conway L (1980) Introduction to VLSI systems. Addison Wesley, Reading, MA
38. Hodges DA, Jackson HG, Saleh R (2003) Analysis and Design of Digital Integrated Circuits. McGraw-Hill, New York
39. Rbaey JM, Chandrakasan A, Nikolic B (1996) Digital Integrated Circuits. Prentice Hall, Englewood Cliffs, NJ
40. Huelsman LP (1972) Basic Circuit Theory with Digital Computations. Prentice-Hall, Englewood Cliffs, NJ
41. Maini AK (1998) Electronic Projects for Beginners. Pustak Mahal, India
42. Zorpette G (2005) Super charged: a tiny South Korean company is out to make capacitors powerful enough to propel the next generation of hybrid-electric cars. IEEE Spectrum 42:32 –37
43. Carpick RW, Sasaki DY, Marcus MS, Eriksson MA, Burns AR (2004) Polydiacetylene films: a review of recent investigations into chromogenic transitions and nanomechanical properties. Journal of Physics-Condensed Matter 16:R679–R697
44. Murugaraj P, Mainwaring D, Mora-Huertas N (2006) Thermistor behaviour in a semiconducting polymer-nanoparticle composite film. Journal of Physics D-Applied Physics 39:2072–2078
45. Chen WX, Lee JY, Liu ZL (2002) Electrochemical lithiation and de-lithiation of carbon nanotube-Sn_2Sb nanocomposites. Electrochemistry Communications 4:260–265
46. batteryuniversity.com.
47. http://en.wikipedia.org.
48. Dang ZM, Wang HY, Zhang YH, Qi JQ (2005) Morphology and dielectric property of homogenous $BaTiO_3$/PVDF nanocomposites prepared via the natural adsorption action of nanosized $BaTiO_3$. Macromolecular Rapid Communications 26:1185–1189
49. Das D, Chakravorty D (2001) Alternating current conductivity of the interfacial phase in copper oxide-silica gel nanocomposites. Journal of Materials Research 16:1047–1051
50. Gonon P, Boudefel A (2006) Electrical properties of epoxy/silver nanocomposites. Journal of Applied Physics 99
51. Li L, Takahashi A, Hao JJ, Kikuchi R, Hayakawa T, Tsurumi TA, Kakimoto MA (2005) Novel polymer-ceramic nanocomposite based on new concepts for embedded capacitor application (I). IEEE Transactions on Components and Packaging Technologies 28:754–759
52. Misman O, Bhattacharya SK, Erbil A, Tummala RR (2000) PWB compatible high value integral capacitors by MOCVD. Journal of Materials Science-Materials in Electronics 11:657–660
53. Pothukuchi S, Li Y, Wong CP (2004) Development of a novel polymer-metal nanocomposite obtained through the route of in situ reduction for integral capacitor application. Journal of Applied Polymer Science 93:1531–1538
54. Rao Y, Ogitani S, Kohl P, Wong CP (2002) Novel polymer-ceramic nanocomposite based on high dielectric constant epoxy formula for embedded capacitor application. Journal of Applied Polymer Science 83:1084–1090
55. Jillek W, Yung WKC (2005) Embedded components in printed circuit boards: a processing technology review. International Journal of Advanced Manufacturing Technology 25:350–360
56. Tummala RR, Rymaszewski EJ, Klopfenstein AG (1999) Microelectronics Packaging Handbook. Kluwer, Norwell
57. Clearfield HM, Wijeyesekera S, Logan EA, Luu A, Gieser D, Lin CM, Jing J (1998) Integrated passive devices using Al/BCB thin films. In Third Advanced Technology on Workshop Integrated Passives Technol, Denver
58. Cho YH, Park JM, Park YH (2004) Preparation and properties of polyimides having highly flexible linkages and their nanocomposites with organoclays. Macromolecular Research 12:38–45
59. Ramesh S, Shutzberg BA, Huang C, Gao J, Giannelis EP (2003) Dielectric nanocomposites for integral thin film capacitors: Materials design, fabrication, and integration issues. IEEE Transactions on Advanced Packaging 26:17–24

60. Rao Y, Wong CP (2004) Material characterization of a high-dielectric-constant polymer-ceramic composite for embedded capacitor for RF applications. Journal of Applied Polymer Science 92:2228–2231
61. Godovski, Yu D (1995) Advances in Polymer Science 119:79–122
62. www.3m.com/us/electronics_mfg/microelectronic_packaging/materials.
63. Rao Y, Yue J, Wong CP (2001) High K polymer-ceramic nano-composite development, characterization and modeling for embedded capacitor RF application. Proceedings of the Electronic Components Technology Conference, 1408–1419
64. Kuo DH, Chang CC, Su TY, Wang WK, Lin BY (2004) Dielectric properties of three ceramic/epoxy composites. Materials Chemistry and Physics 85:201–206
65. Bidstrup-Allen SA, Kohl PA (2002) IEEE Transactions on Advanced Packaging 23:313
66. Vrejoiu I, Pedarnig JD, Dinescu M, Bauer-Gogonea S, Bauerle D (2002) Flexible ceramic-polymer composite films with temperature-insensitive and tunable dielectric permittivity. Applied Physics A-Materials Science & Processing 74:407–409
67. Xu J, Bhattacharya S, Moon K, Lu J, Englert B, Wong CP, Pramanik P (2006) Large Area Processable High k Nanocomposite-Based Embedded Capacitors. IEEE Electronic Components and Technology Proceedings 56:1520–1532
68. Bai Y, Cheng ZY, Bharti V, Xu HS, Zhang QM (2000) High-dielectric-constant ceramic-powder polymer composites. Applied Physics Letters 76:3804–3806
69. Chiteme C, McLachlan DS (2003) ac and dc conductivity, magnetoresistance, and scaling in cellular percolation systems. Physical Review B 67(2), pp. 024206.1–024206.18
70. Desurvire E (1994) Erbium Doped Fiber Amplifiers. Wiley, New York
71. Kozeki M (2002) The condensor film and its property. Proceeding of Eighth JIEP Microfabrication Research Report, 31
72. NEMI (1998) National Electronics Manufacturing Technology Roadmap. National Electronics Manufacturing Initiative, Herndon
73. Chahal P, Tummala R, Allen M, Swaminathan M (1999) IEEE Transactions on Components, Packaging and Manufacturing Technology B21:184
74. Rao Y, Wong CP (2002) Proceedings of the Eight International Symposium on Advanced Packaging Materials, 243
75. Bergman DJ, Stroud D (1992) Physical properties of macroscopically inhomogenous media. Solid State Physics 46:147
76. Clerc JP, Giraud G, Laugier JM, Luck JM (1990) Advances in Physics 39:191
77. Choi SH, Kim JS, Yoon YS (2004) Fabrication and characterization of SnO_2-RuO_2 composite anode thin film for lithium ion batteries. Electrochimica Acta 50:547–552
78. Pecharroman C, Esteban-Betegon F, Bartolome JF, Lopez-Esteban S, Moya JS (2001) New percolative $BaTiO_3$-Ni composites with a high and frequency-independent dielectric constant (epsilon(r) approximate to 80,000). Advanced Materials 13:1541–1544
79. Dang ZM, Shen Y, Nan CW (2002) Dielectric behavior of three-phase percolative Ni–$BaTiO_3$/polyvinylidene fluoride composites. Applied Physics Letters 81:4814–4816
80. Chou YC, Jaw TS (1988) Divergence of dielectric-constant near the percolation-threshold. Solid State Communications 67:753–756
81. Chung KT, Sabo A, Pica AP (1982) Electrical permittivity and conductivity of carbon-black polyvinyl-chloride composites. Journal of Applied Physics 53:6867–6879
82. Grannan DM, Garland JC, Tanner DB (1981) Critical-behavior of the dielectric-constant of a random composite near the percolation-threshold. Physical Review Letters 46:375–378
83. Flandin L, Prasse T, Schueler R, Schulte K, Bauhofer W, Cavaille JY (1999) Anomalous percolation transition in carbon-black-epoxy composite materials. Physical Review B 59: 14349–14355
84. McLachlan DS, Heaney MB (1999) Complex ac conductivity of a carbon black composite as a function of frequency, composition, and temperature. Physical Review B 60:12746–12751
85. Bhattacharyya SK, Basu S, DE SK (1975) Composites Part A-Applied Science and Manufacturing 9:177

86. Luechinger N, Wendelin JS, Bandyopadhyay S, Heness G (2006) Processing, Structure and Electrical Properties of C/Co-Polymer Nanocomposites. Internal Report ETH Zurich/UNSW/UTS
87. Cho SD, Lee JY, Hyun JG, Paik KW (2004) Study on epoxy/$BaTiO_3$ composite embedded capacitor films (ECFs) for organic substrate applications. Materials Science and Engineering B-Solid State Materials for Advanced Technology 110:233–239
88. Dong LJ, Xiong CX, Chen J, Nan CW (2004) Dielectric behavior of $BaTiO_3$/PVDF nanocomposites *in-situ* synthesized by the sol-gel method. Journal of Wuhan University of Technology-Materials Science Edition 19:9–11
89. Wang J, Guo ZP, Zhong S, Liu HK, Dou SX (2003) Lead-coated glass fibre mesh grids for lead-acid batteries. Journal of Applied Electrochemistry 33:1057–1061
90. Wang J, Zhong S, Liu HK, Dou SX (2003) Beneficial effects of red lead on non-cured plates for lead-acid batteries. Journal of Power Sources 113:371–375
91. Chen J, Bradhurst DH, Dou SX, Liu HK (1998) Electrode properties of Mg_2Ni alloy ball-milled with cobalt powder. Electrochimica Acta 44:353–355
92. Luan B, Liu HK, Dou SX (1997) On the elemental substitutions of titanium-based hydrogen-storage alloy electrodes for rechargeable Ni-MH batteries. Journal of Materials Science 32:2629–2635
93. Sadoway DR, Mayes AM (2002) Portable power: advanced rechargeable lithium batteries. Mrs Bulletin 27:590–592
94. Liu HK, Wang GX, Guo ZP, Wang JZ, Konstantinov K (2006) Nanomaterials for lithium-ion rechargeable batteries. Journal of Nanoscience and Nanotechnology 6:1–15
95. Ng SH, Wang J, Konstantinov K, Wexler D, Chen J, Liu HK (2006) Spray pyrolyzed PbO–carbon nanocomposites as anode for lithium-ion batteries. Journal of the Electrochemical Society 153:A787–A793
96. Selvan RK, Kalaiselvi N, Augustin CO, Doh CH, Sanjeeviraja C (2006) $CuFe_2O_4/SnO_2$ nanocomposites as anodes for Li-ion batteries. Journal of Power Sources 157:522–527
97. Huggins RA (2002) Alternative materials for negative electrodes in lithium systems. Solid State Ionics 152:61–68
98. Winter M, Brodd RJ (2004) What are batteries, fuel cells, and supercapacitors? Chemical Reviews 104:4245–4269
99. Scrosati B (1992) Lithium rocking chair batteries – an old concept. Journal of the Electrochemical Society 139:2776–2781
100. Besenhard JO, Wagner MW, Winter M, Jannakoudakis AD, Jannakoudakis PD, Theodoridou E (1993) Inorganic film-forming electrolyte additives improving the cycling behavior of metallic lithium electrodes and the self-discharge of carbon lithium electrodes. Journal of Power Sources 44:413–420
101. Imanishi N, Kashiwagi H, Ichikawa T, Takeda Y, Yamamoto O, Inagaki M (1993) Charge-discharge characteristics of mesophase-pitch-based carbon-fibers for lithium cells. Journal of the Electrochemical Society 140:315–320
102. Ahn JH, Wang GX, Yao J, Liu HK, Dou SX (2003) Tin-based composite materials as anode materials for Li-ion batteries. Journal of Power Sources 119:45–49
103. Hibino M, Abe K, Mochizuki M, Miyayama M (2004) Amorphous titanium oxide electrode for high-rate discharge and charge. Journal of Power Sources 126:139–143
104. Poizot P, Laruelle S, Grugeon S, Dupont L, Tarascon J-M (2000) Nature 407:496–499
105. Sides CR, Martin CR (2005) Nanostructured electrodes and the low-temperature performance of Li-ion batteries. Advanced Materials 17:125–128
106. Cheng XQ, Shi PF (2005) Electroless Cu-plated Ni_3Sn_4 alloy used as anode material for lithium ion battery. Journal of Alloys and Compounds 391:241–244
107. Kim YU, Lee SI, Lee CK, Sohn HJ (2005) Enhancement of capacity and cycle-life of $Sn_{+delta}P_3$ (0 <= delta <= 1) anode for lithium secondary batteries. Journal of Power Sources 141:163–166
108. Xie J, Zhao XB, Cao GS, Zhong YD, Zhao MJ, Tu JP (2005) Solvothermal synthesis of nanosized $CoSb_2$ alloy anode for Li-ion batteries. Electrochimica Acta 50:1903–1907

109. Reddy MV, Wannek C, Pecquenard B, Vinatier P, Levasseur A (2003) $LiNiVO_4$-promising thin films for use as anode material in microbatteries. Journal of Power Sources 119:101–105
110. Idota Y, Kubota T, Matsufuji A, Maekawa Y, Miyasaka T (1997) Tin-based amorphous oxide: A high-capacity lithium-ion-storage material. Science 276:1395–1397
111. Nishijima M, Takeda Y, Imanishi N, Yamamota O (1994) Li deintercalation and structural change in the lithium transition metal nitride Li_3FeN_2. Journal of Solid State Chemistry 113:205–210
112. Kishore M, Varadaraju UV, Raveau B (2004) Electrochemical performance of LiMSnO (M = Fe, In) phases with ramsdellite structure as anodes for lithium batteries. Journal of Solid State Chemistry 177:3981–3986
113. Kalaiselvi N, Doh CH, Park CW, Moon SI, Yun MS (2004) A novel approach to exploit $LiFePO_4$ compound as an ambient temperature high capacity anode material for rechargeable lithium batteries. Electrochemistry Communications 6:1110–1113
114. Son JT (2004) Novel electrode material for Li ion battery based on polycrystalline $LiNbO_3$. Electrochemistry Communications 6:990–994
115. Chu YQ, Fu ZW, Qin QZ (2004) Cobalt ferrite thin films as anode material for lithium ion batteries. Electrochimica Acta 49:4915–4921
116. Alcantara R, Jaraba M, Lavela P, Tirado JL, Jumas JC, Olivier-Fourcade J (2003) Changes in oxidation state and magnetic order of iron atoms during the electrochemical reaction of lithium with $NiFe_2O_4$. Electrochemistry Communications 5:16–21
117. NuLi YN, Qin QZ (2005) Nanocrystalline transition metal ferrite thin films prepared by an electrochemical route for Li-ion batteries. Journal of Power Sources 142:292–297
118. NuLi YN, Chu YQ, Qin QZ (2004) Nanocrystalline $ZnFe_2O_4$ and Ag-doped $ZnFe_2O_4$ films used as new anode materials for Li-ion batteries. Journal of the Electrochemical Society 151:A1077–A1083
119. Sharma N, Shaju KM, Rao GVS, Chowdari BVR (2003) Iron-tin oxides with $CaFe_2O_4$ structure as anodes for Li-ion batteries. Journal of Power Sources 124:204–212
120. Idota Y, Mishima M, Miyaki Y, Kubota T, Miyasaki T (1994) Canadian Patent Application 2:134
121. Idota Y, Mishima M (1995) Canadian Patent Application 2:143
122. Brousse T, Retoux R, Herterich U, Schleich DM (1998) Thin-film crystalline SnO_2-lithium electrodes. Journal of the Electrochemical Society 145:1–4
123. Courtney IA, McKinnon WR, Dahn JR (1999) On the aggregation of tin in SnO composite glasses caused by the reversible reaction with lithium. Journal of the Electrochemical Society 146:59–68
124. Goward GR, Leroux F, Power WP, Ouvrard G, Dmowski W, Egami T, Nazar LF (1999) On the nature of Li insertion in tin composite oxide glasses. Electrochemical and Solid State Letters 2:367–370
125. Liu W, Huang X, Wang Z, Li H, Chen L (1998) J. Electrochem. Soc. 145:59
126. Wolfenstine J, Sakamoto J, Huang CK (1998) Tin oxide tin composite anodes for use in Li-ion batteries. Journal of Power Sources 75:181–182
127. Courtney IA, Dahn JR (1997) Electrochemical and in situ X-ray diffraction studies of the reaction of lithium with tin oxide composites. Journal of the Electrochemical Society 144:2045–2052
128. Cruz M, Hernan L, Morales J, Sanchez L (2002) Spray pyrolysis as a method for preparing PbO coatings amenable to use in lead-acid batteries. Journal of Power Sources 108:35–40
129. Martos M, Morales J, Sanchez L, Ayouchi R, Leinen D, Martin F, Barrado JRR (2001) Electrochemical properties of lead oxide films obtained by spray pyrolysis as negative electrodes for lithium secondary batteries. Electrochimica Acta 46:2939–2948
130. Yang J, Winter M, Besenhard JO (1996) Small particle size multiphase Li-alloy anodes for lithium-ion-batteries. Solid State Ionics 90:281–287
131. Huggins RA (1999) Lithium alloy negative electrodes. Journal of Power Sources 82:13–19
132. Mao O, Turner RL, Courtney IA, Fredericksen BD, Buckett MI, Krause LJ, Dahn JR (1999) Active/inactive nanocomposites as anodes for Li-ion batteries. Electrochemical and Solid State Letters 2:3–5

133. Yang J, Wachtler M, Winter M, Besenhard JO (1999) Sub-microcrystalline Sn and Sn-SnSb powders as lithium storage materials for lithium-ion batteries. Electrochemical and Solid State Letters 2:161–163
134. Li NC, Martin CR (2001) A high-rate, high-capacity, nanostructured Sn-based anode prepared using sol–gel template synthesis. Journal of the Electrochemical Society 148:A164–A170
135. Li NC, Martin CR, Scrosati B (2000) A high-rate, high-capacity, nanostructured tin oxide electrode. Electrochemical and Solid State Letters 3:316–318
136. Whitehead AH, Elliott JM, Owen JR (1999) Nanostructured tin for use as a negative electrode material in Li-ion batteries. Journal of Power Sources 82:33–38
137. Yang J, Takeda Y, Imanishi N, Yamamoto O (1999) Ultrafine Sn and $SnSb_{0.14}$ powders for lithium storage matrices in lithium-ion batteries. Journal of the Electrochemical Society 146:4009–4013
138. Yang J, Takeda Y, Imanishi N, Ichikawa T, Yamamoto O (1999) Study of the cycling performance of finely dispersed lithium alloy composite electrodes under high Li-utilization. Journal of Power Sources 79:220–224
139. Che GL, Lakshmi BB, Fisher ER, Martin CR (1998) Carbon nanotubule membranes for electrochemical energy storage and production. Nature 393:346–349
140. Dahn JR, Zheng T, Liu YH, Xue JS (1995) Mechanisms for lithium insertion in carbonaceous materials. Science 270:590–593
141. Gao B, Kleinhammes A, Tang XP, Bower C, Fleming L, Wu Y, Zhou O (1999) Electrochemical intercalation of single-walled carbon nanotubes with lithium. Chemical Physics Letters 307:153–157
142. Guo ZP, Zhao ZW, Liu HK, Dou SX (2005) Electrochemical lithiation and de-lithiation of MWNT-Sn/SnNi nanocomposites. Carbon 43:1392–1399
143. Tans SJ, Verschueren ARM, Dekker C (1998) Room-temperature transistor based on a single carbon nanotube. Nature 393:49–52
144. Wang GX, Yao J, Liu HK (2004) Characterization of nanocrystalline Si-MCMB composite anode materials. Electrochemical and Solid State Letters 7:A250–A253
145. Badway F, Pereira N, Cosandey F, Amatucci GG (2003) Carbon-metal fluoride nanocomposites – structure and electrochemistry of FeF_3:C. Journal of the Electrochemical Society 150:A1209–A1218
146. Wang Y, Lee JY (2005) Microwave-assisted synthesis of SnO_2-graphite nanocomposites for Li-ion battery applications. Journal of Power Sources 144:220–225
147. Fleischauer MD, Topple JM, Dahna JR (2005) Combinatorial investigations of Si–M (M = Cr plus Ni, Fe, Mn) thin film negative electrode materials. Electrochemical and Solid State Letters 8:A137–A140
148. Li H, Huang XJ, Chen LQ, Wu ZG, Liang Y (1999) Electrochemical and Solid-State Letters 2:547
149. http://www.physorg.com/news3061.html.
150. Nalimova VA, Sklovsky DE, Bondarenko GN, Alvergnat-Gaucher H, Bonnamy S, Beguin F (1997) Lithium interaction with carbon nanotubes. Synthetic Metals 88:89–93
151. Claye AS, Fischer JE, Huffman CB, Rinzler AG, Smalley RE (2000) Solid-state electrochemistry of the Li single wall carbon nanotube system. Journal of the Electrochemical Society 147:2845–2852
152. Frackowiak E, Gautier S, Gaucher H, Bonnamy S, Beguin F (1999) Electrochemical storage of lithium multiwalled carbon nanotubes. Carbon 37:61–69
153. Kim I, Kumta PN, Blomgren GE (2000) Si/TiN nanocomposites – novel anode materials for Li-ion batteries. Electrochemical and Solid State Letters 3:493–496
154. Lee KT, Jung YS, Oh SM (2003) Synthesis of tin-encapsulated spherical hollow carbon for anode material in lithium secondary batteries. Journal of the American Chemical Society 125:5652–5653
155. Besenhard JO (1999) Handbook of Battery Materials. Wiley VCH, Weinheim
156. Fu LJ, Liu H, Zhang HP, Li C, Zhang T, Wu YP, Holze R, Wu HQ (2006) Synthesis and electrochemical performance of novel core/shell structured nanocomposites. Electrochemistry Communications 8:1–4

157. Wang GX, Ahn JH, Yao J, Bewlay S, Liu HK (2004) Nanostructured Si-C composite anodes for lithium-ion batteries. Electrochemistry Communications 6:689–692
158. Wang GX, Chen Y, Yang L, Yao J, Needham S, Liu HK, Ahn JH (2005) Journal Power Sources 146:487
159. Martos M, Morales J, Sanchez L (2003) Lead-based systems as suitable anode materials for Li-ion batteries. Electrochimica Acta 48:615–621
160. Yuan L, Konstantinov K, Wang GX, Liu HK, Dou SX (2005) Nano-structured SnO_2-carbon composites obtained by in situ spray pyrolysis method as anodes in lithium batteries. Journal of Power Sources 146:180–184
161. Bewlay SL, Konstantinov K, Wang GX, Dou SX, Liu HK (2004) Conductivity improvements to spray-produced $LiFePO_4$ by addition of a carbon source. Materials Letters 58: 1788–1791
162. Yoshio M, Wang HY, Fukuda K, Umeno T, Dimov N, Ogumi Z (2002) Carbon-coated Si as a lithium-ion battery anode material. Journal of the Electrochemical Society 149:A1598–A1603
163. Kim Y, Goh WH, Chang T, Ha CS, Ree M (2004) Optical and dielectric anisotropy in polyimide nanocomposite films prepared from soluble poly(amic diethyl ester) precursors. Advanced Engineering Materials 6:39–43
164. Yu J, Ree M, Shin TJ, Park YH, Cai W, Zhou D, Lee KW (2000) Adhesion of poly (4,4′-oxydiphenylene pyromellitimide) to copper metal using a polymeric primer: Effects of miscibility and polyimide precursor origin. Macromolecular Chemistry and Physics 201:491–499
165. Wu YP, Dai XB, Ma JQ, Chen YJ (2004) Lithium Ion Batteries – Practice and Applications. Chemical Industry Press, Beijing
166. Wilson AM, Dahn JR (1995) Lithium Insertion in Carbons Containing Nanodispersed Silicon. Journal of the Electrochemical Society 142:326–332
167. Gratz J, Ahn CC, Yazami R, Fultz B, A194. (1999) Electrochemical Solid-state lett ers 6:A 194
168. Ohara S, Suzuki J, Sekine K, Takamura T (2003) Li insertion/extraction reaction at a Si film evaporated on a Ni foil. Journal of Power Sources 119:591–596
169. Niu J, Lee JY (2002) Electrochemical Solid-State Letters 5:A107
170. Wang CS, Wu GT, Zhang XB, Qi ZF, Li WZ (1998) Lithium insertion in carbon-silicon composite materials produced by mechanical milling. Journal of the Electrochemical Society 145:2751–2758
171. Menard E, Lee KJ, Khang DY, Nuzzo RG, Rogers JA (2004) A printable form of silicon for high performance thin film transistors on plastic substrates. Applied Physics Letters 84:5398–5400
172. Chan VZH, Hoffman J, Lee VY, Iatrou H, Avgeropoulos A, Hadjichristidis N, Miller RD, Thomas EL (1999) Ordered bicontinuous nanoporous and nanorelief ceramic films from self assembling polymer precursors. Science 286:1716–1719
173. Maex K, Baklanov MR, Shamiryan D, Iacopi F, Brongersma SH, Yanovitskaya ZS (2003) Low dielectric constant materials for microelectronics. Journal of Applied Physics 93:8793–8841
174. Morgen M, Ryan ET, Zhao JH, Hu C, Cho TH, Ho PS (2000) Low dielectric constant materials for ULSI interconnects. Annual Review of Materials Science 30:645–680
175. Semiconductor Industry Association (2004) International Technology Roadmap for Semiconductors. Semiconductor Industry Association, San Jose
176. Ho PKH, Friend RH (2002) pi-electronic and electrical transport properties of conjugated polymer nanocomposites: Poly(*p*-phenylenevinylene) with homogeneously dispersed silica nanoparticles. Journal of Chemical Physics 116:6782–6794
177. Maier G (2001) Low dielectric constant polymers for microelectronics. Progress in Polymer Science 26:3–65
178. Moylan CR, Best ME, Ree M (1991) Solubility of water in polyimides – quartz crystal microbalance measurements. Journal of Polymer Science Part B-Polymer Physics 29:87–92
179. Carter KR, DiPietro RA, Sanchez MI, Russell TP, Lakshmanan P, McGrath JE (1997) Polyimide nanofoams based on ordered polyimides derived from poly(amic alkyl esters): PMDA/4-BDAF. Chemistry of Materials 9:105–118

180. Carter KR, DiPietro RA, Sanchez MI, Swanson SA (2001) Nanoporous polyimides derived from highly fluorinated polyimide/poly(propylene oxide) copolymers. Chemistry of Materials 13:213–221
181. Mikoshiba S, Hayase S (1999) Preparation of low density poly(methylsilsesquioxane)s for LSI interlayer dielectrics with low dielectric constant. Fabrication of angstrom size pores prepared by baking trifluoropropylsilyl copolymers. Journal of Materials Chemistry 9:591–598
182. Azzam RMA, Bashara NM (1977) Ellipsometry and Polarized Light. North-Holland, Amsterdam
183. Licata TJ, Colgan EG, Harper JME, Luce SE (1995) Interconnect fabrication processes and the development of low-cost wiring for CMOS products. IBM Journal of Research and Development 39:419–435
184. Lee YJ, Huang JM, Kuo SW, Chang FC (2005) Low-dielectric, nanoporous polyimide films prepared from PEO-POSS nanoparticles. Polymer 46:10056–10065
185. Chen GZ, Shaffer MSP, Coleby D, Dixon G, Zhou WZ, Fray DJ, Windle AH (2000) Carbon nanotube and polypyrrole composites: coating and doping. Advanced Materials 12:522–526
186. Curran SA, Ajayan PM, Blau WJ, Carroll DL, Coleman JN, Dalton AB, Davey AP, Drury A, McCarthy B, Maier S, Strevens A (1998) A composite from poly(m-phenylenevinylene-co-2,5-dioctoxy-*p*-phenylenevinylene) and carbon nanotubes: A novel material for molecular optoelectronics. Advanced Materials 10:1091–1093
187. Dai L (1999) Effective bandwidths and performance bounds in high-speed communication systems. Journal of Optimization Theory and Applications 100:549–574
188. Saito Y, Uemura S, Hamaguchi K (1998) Cathode ray tube lighting elements with carbon nanotube field emitters. Japanese Journal of Applied Physics Part 2-Letters & Express Letters 37:L346–L348
189. Downs C, Nugent J, Ajayan PM, Duquette DJ, Santhanam SV (1999) Efficient polymerization of aniline at carbon nanotube electrodes. Advanced Materials 11:1028–1031
190. Valter B, Ram MK, Nicolini C (2002) Synthesis of multiwalled carbon nanotubes and poly(o-anisidine) nanocomposite material: Fabrication and characterization of its Langmuir-Schaefer films. Langmuir 18:1535–1541
191. Zengin H, Zhou WS, Jin JY, Czerw R, Smith DW, Echegoyen L, Carroll DL, Foulger SH, Ballato J (2002) Carbon nanotube doped polyaniline. Advanced Materials 14:1480–1483
192. Coleman JN, Curran S, Dalton AB, Davey AP, McCarthy B, Blau W, Barklie RC (1998) Percolation-dominated conductivity in a conjugated-polymer-carbon-nanotube composite. Physical Review B 58:R7492–R7495
193. Lefrant S, Baibarac M, Baltog I, Godon C, Mevellec JY, Wery J, Faulques E, Mihut L, Aarab H, Chauvet O (2005) SERS, FT-IR and photoluminescence studies on single-walled carbon nanotubes/conducting polymers composites. Synthetic Metals 155:666–669
194. Woo HS, Czerw R, Webster S, Carroll DL, Park JW, Lee JH (2001) Organic light emitting diodes fabricated with single wall carbon nanotubes dispersed in a hole conducting buffer: the role of carbon nanotubes in a hole conducting polymer. Synthetic Metals 116:369–372
195. Kymakis E, Amaratunga GAJ (2002) Single-wall carbon nanotube/conjugated polymer photovoltaic devices. Applied Physics Letters 80:112–114
196. Woo HS, Kim YB, Czerw R, Carroll DL, Ballato J, Ajayan PM (2004) Tailoring hole transport in organic light-emitting devices using carbon nanotube-polymer nanocomposites. Journal of the Korean Physical Society 45:507–511
197. Star A, Stoddart JF, Steuerman D, Diehl M, Boukai A, Wong EW, Yang X, Chung SW, Choi H, Heath JR (2001) Preparation and properties of polymer-wrapped single-walled carbon nanotubes. Angewandte Chemie-International Edition 40:1721–1725
198. Qi PF, Javey A, Rolandi M, Wang Q, Yenilmez E, Dai HJ (2004) Miniature organic transistors with carbon nanotubes as quasi-one-dimensional electrodes. Journal of the American Chemical Society 126:11774–11775
199. Bachtold A, Hadley P, Nakanishi T, Dekker C (2001) Logic circuits with carbon nanotube transistors. Science 294:1317–1320

200. Postma HWC, Teepen T, Yao Z, Grifoni M, Dekker C (2001) Carbon nanotube single-electron transistors at room temperature. Science 293:76–79
201. Yao Z, Dekker C, Avouris P (2001) Carbon Nanotubes. 80:147–171
202. Duan XF, Huang Y, Lieber CM (2002) Nano Letters 2:487–490
203. Ouyang M, Huang JL, Cheung CL, Lieber CM (2001) Science 291:97–100
204. Rueckes T, Kim K, Joselevich E, Tseng GY, Cheung CL, Lieber CM (2000) Science 289:94–97
205. Avouris P (2002) Molecular Electronics with Carbon Nanotubes. Accounts of Chemical Research 35:1026–1034
206. Liu J, Rinzler AG, Dai HJ, Hafner JH, Bradley RK, Boul PJ, Lu A, Iverson T, Shelimov K, Huffman CB, Rodriguez-Macias F, Shon YS, Lee TR, Colbert DT, Smalley RE (1998) Fullerene pipes. Science 280:1253–1256
207. Banerjee S, Wong SS (2002) Functionalization of carbon nanotubes with a metal-containing molecular complex. Nano Letters 2:49–53
208. Banerjee S, Wong SS (2002) Structural characterization, optical properties, and improved solubility of carbon nanotubes functionalized with Wilkinson's catalyst. Journal of the American Chemical Society 124:8940–8948
209. Banerjee S, Wong SS (2002) Synthesis and characterization of carbon nanotube-nanocrystal heterostructures. Nano Letters 2:195–200
210. Dimitrakopoulos CD, Mascaro DJ (2001) Organic thin-film transistors: a review of recent advances. IBM Journal of Research and Development 45:11–27
211. Lodha A, Singh R (2001) Prospects of manufacturing organic semiconductor-based integrated circuits. IEEE Transactions on Semiconductor Manufacturing 14:281–296
212. Martel R, Schmidt T, Shea HR, Hertel T, Avouris P (1998) Single- and multi-wall carbon nanotube field-effect transistors. Applied Physics Letters 73:2447–2449
213. Ramamurthy PC, Malshe AM, Harrell WR, Gregory RV, McGuire K, Rao AM (2004) Polyaniline/single-walled carbon nanotube composite electronic devices. Solid-State Electronics 48:2019–2024
214. Kuo CT, Chiou WH (1997) Field-effect transistor with polyaniline thin film as semiconductor. Synthetic Metals 88:23–30
215. Javey A, Guo J, Paulsson M, Wang Q, Mann D, Lundstrom M, Dai HJ (2004) High-field quasiballistic transport in short carbon nanotubes. Physical Review Letters 92(10): 106804/1–4
216. Snow ES, Novak JP, Lay MD, Houser EH, Perkins FK, Campbell PM (2004) Carbon nanotube networks: Nanomaterial for macroelectronic applications. Journal of Vacuum Science & Technology B 22:1990–1994
217. Seidel R, Graham AP, Unger E, Duesberg GS, Liebau M, Steinhoegl W, Kreupl F, Hoenlein W (2004) High-current nanotube transistors. Nano Letters 4:831–834
218. Seidel RV, Graham AP, Rajasekharan B, Unger E, Liebau M, Duesberg GS, Kreupl F, Hoenlein W (2004) Bias dependence and electrical breakdown of small diameter single-walled carbon nanotubes. Journal of Applied Physics 96:6694–6699
219. Tsvetkov MY, Kleshcheva SM, Samoilovich MI, Gaponenko NV, Shushunov AN (2005) Erbium photoluminescence in opal matrix and porous anodic alumina nanocomposites. Microelectronic Engineering 81:273–280
220. Suzuki N, Tomita Y (2003) Diffraction properties of volume holograms recorded in SiO_2 nanoparticle-dispersed methacrylate photopolymer films. Japanese Journal of Applied Physics Part 2-Letters 42:L927–L929
221. Siwick BJ, Kalinina O, Kumacheva E, Miller RJD, Noolandi J (2001) Polymeric nanostructured material for high-density three-dimensional optical memory storage. Journal of Applied Physics 90:5328–5334
222. Parthenopoulous DA, Rentzepis PM (1989) Science 245:843
223. Caruso RA, Antonietti M (2001) Sol–gel nanocoating: an approach to the preparation of structured materials. Chemistry of Materials 13:3272–3282

224. Kawata S, Kawata Y (2000) Three-dimensional optical data storage using photochromic materials. Chemical Reviews 100:1777–1788
225. Malini KA, Anantharaman MR, Sindhu S, Chinnasamy CN, Ponpandian N, Narayanasamy A, Balachandran M, Pillai VNS (2001) Effect of cycling on the magnetization of ion exchanged magnetic nanocomposite based on polystyrene. Journal of Materials Science 36:821–824
226. Suzuki N, Tomita Y (2006) Highly transparent ZrO_2 nanoparticle-dispersed acrylate photopolymers for volume holographic recording. Optics Express 14:12712–12719
227. Kalinina O, Kumacheva E (2001) Nanostructured polymer films with liquid inclusions. 1. Structural blocks. Macromolecules 34:6380–6386
228. Kim E, Park J, Shin C, Kim N (2006) Effect of organic side-chains on the diffraction efficiency of an organic-inorganic hybrid nanocomposite film. Nanotechnology 17:2899–2906
229. Judeinstein P, Oliveira PW, Krug H, Schmidt H (1997) Photochromic organic-inorganic nanocomposites as holographic storage media. Advanced Materials for Optics and Electronics 7:123–133
230. Trentler TJ, Boyd JE, Colvin VL (2000) Epoxy resin-photopolymer composites for volume holography. Chemistry of Materials 12:1431–1438
231. Suzuki N, Tomita Y (2004) Silica-nanoparticle-dispersed methacrylate photopolymers with net diffraction efficiency near 100%. Applied Optics 43:2125–2129
232. Suzuki N, Tomita Y, Kojima T (2002) Holographic recording in TiO_2 nanoparticle-dispersed methacrylate photopolymer films. Applied Physics Letters 81:4121–4123
233. Tomita Y, Nishibiraki H (2003) Improvement of holographic recording sensitivities in the green in SiO_2 nanoparticle-dispersed methacrylate photopolymers doped with pyromethene dyes. Applied Physics Letters 83:410–412
234. Sanchez C, Escuti MJ, van Heesch C, Bastiaansen CWM, Broer DJ, Loos J, Nussbaumer R (2005) TiO_2 nanoparticle-photopolymer holographic recording. Advanced Functional Materials 15:1623–1629
235. Koshida N, Gelloz B (1999) Wet and dry porous silicon. Current Opinion in Colloid & Interface Science 4:309–313
236. Altukhov PD, Kuzminov EG (1999) Condensation of a hot electron-hole plasma in tunneling silicon MOS structures. Solid State Communications 111:379–384
237. Green MA, Zhao JH, Wang AH, Reece PJ, Gal M (2001) Efficient silicon light-emitting diodes. Nature 412:805–808
238. Pavesi L, Dal Negro L, Mazzoleni C, Franzo G, Priolo F (2000) Optical gain in silicon nanocrystals. Nature 408:440–444
239. Simons AJ, Cox TI, Loni A, Canham LT, Blacker R (1997) Investigation of the mechanisms controlling the stability of a porous silicon electroluminescent device. Thin Solid Films 297:281–284
240. Sticht A, Neufeld E, Luigart A, Brunner K, Abstreiter G, Bay H (1998) Characteristics of surface and waveguide emitting SiGe: Er: O diodes. Journal of Luminescence 80:321–327
241. Amato G, Boarino L, Midellino D, Rossi AM (2000) Philosophical Magazine B 80:679
242. Lu ZH, Grozea D (2002) Crystalline Si/SiO_2 quantum wells. Applied Physics Letters 80:255–257
243. Parisini A, Angelucci R, Dori L, Poggi A, Maccagnani P, Cardinali GC, Amato G, Lerondel G, Midellino D (2000) TEM characterisation of porous silicon. Micron 31:223–230
244. Lopez HA, Fauchet PM (2001) Infrared LEDs and microcavities based on erbium-doped silicon nanocomposites. Materials Science and Engineering B-Solid State Materials for Advanced Technology 81:91–96
245. Cristea D, Obreja P, Kusko M, Manea E, Rebigan R (2006) Polymer micromachining for micro- and nanophotonics. Materials Science & Engineering C-Biomimetic and Supramolecular Systems 26:1049–1055
246. Lal M, Kumar ND, Joshi MP, Prasad PN (1998) Polymerization in a reverse micelle nanoreactor: Preparation of processable poly(*p*-phenylenevinylene) with controlled conjugation length. Chemistry of Materials 10:1065–1068

247. Lee J, Cho HJ, Cho NS, Hwang DH, Kang JM, Lim E, Lee JI, Shim HK (2006) Enhanced efficiency of polyfluorene derivatives: Organic-inorganic hybrid polymer light-emitting diodes. Journal of Polymer Science Part A-Polymer Chemistry 44:2943–2954
248. Ho PKH, Kim JS, Tessler N, Friend RH (2001) Photoluminescence of poly(*p*-phenylenevinylene)-silica nanocomposites: Evidence for dual emission by Franck-Condon analysis. Journal of Chemical Physics 115:2709–2720
249. An HY, Chen BJ, Hou JY, Shen JC, Liu SY (1998) Exciton confinement in organic multiple quantum well structures. Journal of Physics D-Applied Physics 31:1144
250. Yang SH, Nguyen TP, Le Rendu P, Hsu CS (2005) Optical and electrical investigations of poly(*p*-phenylene vinylene)/silicon oxide and poly(*p*-phenylene vinylene)/titanium oxide nanocomposites. Thin Solid Films 471:230–235
251. Lee TW, Park OO, Kim JJ, Hong JM, Kim YC (2001) Efficient photoluminescence and electroluminescence from environmentally stable polymer/clay nanocomposites. Chemistry of Materials 13:2217–2222
252. Nguyen T-Q, Wu J, Doan W, Schwartz BJ, Tolbert SH (2000) Science:288
253. Qian L, Zhang T, Wageh S, Jin ZS, Du ZL, Wang YS, Xu XR (2006) Study of blue electroluminescence from titania nanotubes doped into a polymeric matrix. Nanotechnology 17:100–104
254. Lee TW, Park OO, Hong JM, Kim DY, Kim YC (2001) Carrier mobilities of polymer/organo-clay nanocomposite electroluminescent devices. Thin Solid Films 393:347–351
255. Yokozumi T, Kim SH, Washino K, Lee HC, Ogion K, Usui H, Sato H (2003) Semiconducting nanocomposite from titanium dioxide and organic charge transporting compound. Synthetic Metals 139:151–154
256. Lee HC, Lee TW, Lim YT, Park OO (2002) Improved environmental stability in poly(*p*-phenylene vinylene)/layered silicate nanocomposite. Applied Clay Science 21:287–293
257. Lee TW, Park OO, Yoon J, Kim JJ (2001) Enhanced quantum efficiency in polymer/layered silicate nanocomposite light-emitting devices. Synthetic Metals 121:1737–1738
258. Senkevich JJ, Desu SB (1998) Poly(chloro-*p*-xylylene)/SiO_2 multilayer thin films deposited near room temperature by thermal CVD. Thin Solid Films 322:148–157
259. Senkevich JJ, Desu SB (2000) Compositional studies of near-room-temperature thermal CVD poly(chloro-*p*-xylylene)/SiO_2 nanocomposites. Applied Physics A-Materials Science & Processing 70:541–546
260. Ezhilvalavan S, Tseng TY (1999) Preparation and properties of tantalum pentoxide (Ta_2O_5) thin films for ultra large scale integrated circuits (ULSIs) application: A review. Journal of Materials Science: Materials in Electronics 10:9–31
261. Chashechnikova I, Dolgov L, Gavrilko T, Puchkovska G, Shaydyuk Y, Lebovka N, Moraru V, Baran J, Ratajczak H (2005) Optical properties of heterogeneous nanosystems based on montmorillonite clay mineral and 5CB nematic liquid crystal. Journal of Molecular Structure 744–747:563–571
262. Zhu W (2001) Vacuum Microelectronics. Wiley, New York
263. Bajic S, Latham RV (1988) Enhanced cold-cathode emission using composite resin-carbon coatings. Journal of Physics D: Applied Physics 21:200
264. Tsang WM, Stolojan V, Wong SP, Sealy BJ, Silva SRP (2005) The electron field emission properties of ion beam synthesized metal-dielectric nanocomposite layers on silicon substrates. Materials Science and Engineering B-Solid State Materials for Advanced Technology 124:453–457
265. http://www.nanotechproject.org/.